Review

M–N–C materials as heterogeneous catalysts for organic transformations

Kefeng Ping [a,b], Rohit Bhadoria [a,c], Pavel Starkov [a], Nadezda Kongi [d,*]

[a] *Department of Chemistry and Biotechnology, Tallinn University of Technology, Tallinn 12618, Estonia*
[b] *Yichang Humanwell Pharmaceutical Co., Ltd, 19 Dalian Rd, Xiling District, Yichang 443005, Hubei, China*
[c] *Division of Hematology/Oncology, School of Medicine, University of California, San Francisco, San Francisco, CA 94158, United States*
[d] *Institute of Chemistry, University of Tartu, Tartu 50411, Estonia*

ARTICLE INFO

ABSTRACT

M–N–C (metal-nitrogen-carbon) materials have gained recognition as versatile and effective catalysts in heterogeneous catalysis and electrocatalytic reactions. This review provides a comprehensive overview of their reactivity, with a particular emphasis on their use in organic transformations. The review discusses the synthesis of M–N–C materials from organic precursors, and the effect of different precursors on their catalytic activity. Techniques for improving their catalytic activity, such as optimizing their performance in reductions and oxidations, are also discussed. The challenges and limitations associated with the use of M–N–C materials as catalysts, including stability and environmental toxicity, are explored. Despite these challenges, the review underscores the versatility and potential of M–N–C materials as catalysts, and provides insights into future research directions for improving their stability and performance.

1. M–N–C catalyst materials

M–N–C materials, or metal- and nitrogen-doped carbon materials, are a class of materials that have gained widespread use in a variety of applications due to their unique properties [1–5]. These materials are often used as sensors and nanozymes [1,2], and they have also found widespread use in the field of electrocatalysis, where they are used in the development of clean energy storage and conversion technologies, such as rechargeable metal-air batteries, fuel cells, and electrolyzers [1,3–9]. M–N–C catalysts have been widely used in a variety of electrocatalytic conversion reactions, including oxygen reduction reaction (ORR) [10–14], oxygen evolution reaction (OER) [15–18], hydrogen evolution reaction (HER) [19–22], nitrogen reduction reaction (NRR) [1,23–25], and carbon dioxide reduction reaction (CO2RR) [1,20,22,26,27] (Scheme 1).

In addition to their use in electrocatalysis, M–N–C materials have also been employed in heterogeneous catalysis [4,28–33], where they have been used to catalyze a wide range of organic transformations, including reductions, oxidations, which may often be coupled to a secondary process such as amination, condensation, and esterification [34–53]. Much of the research on M–N–C materials has focused on iron- and cobalt-based materials, although other metals, such as nickel, have also been explored.

M–N–C materials are steadily transforming into 'privileged materials' for organic transformations. While in metal and organocatalysis, a number of ligands are referred to as 'privileged ligands' [54], a similar concept of rational selection of organic precursors can be used to fabricate multifunctional catalysts. In this review, we offer a comprehensive assessment of the reactivity of M–N–C catalysts in organic transformations, detailing their optimization and techniques for enhancing their performance.

1.1. Preparation of catalysts

There are two most widely used strategies to fabricate M–N–C catalysts [7,10]. One is based on combining various supports, metal salts and heteroatom dopants. Another strategy relies on using nitrogen-rich metal–organic or metal-doped covalent organic frameworks (MOFs and COFs, respectively). However, **carbonization** by heat treatment in the 400–1000 °C range is always required to increase carbon content and generate active species. Typically, this leads to the formation of metal nanoparticles (NPs) or metal-coordinated sites. The latter is often referred to as single-atom catalysts (SACs) [55,56]. In the more complex, bimetallic systems, additional proposed catalytically active sites include ligated bimetallic sites [57–59], as well as metal alloy nanoparticles [60]. These species may contribute to the overall enhanced catalytic
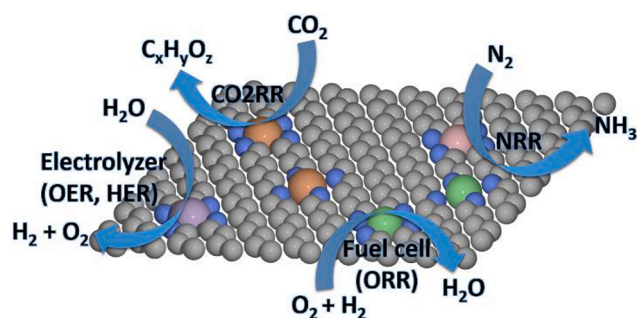
---

* Corresponding author.
 E-mail address: nadezda.kongi@ut.ee (N. Kongi).

Scheme 1. Electrochemical processes employing M–N–C materials.

properties of the underlying materials either independently or synergistically.

In case one prefers to use a **combination** of various precursors (metal salts, supports, dopants) to generate the M–N–C materials, significant consideration should be given to each component's role, including their ratios. For example, there are many **carbon supports** onto which the catalytically active sites can be installed [61]. These include various carbon materials – nanotubes (CNT), activated carbon, Vulcan XC72R, graphene, graphene oxide (GO), reduced graphene oxide (rGO), g-C_3N_4 [62], MXenes [63], and polymers such as polyvinylpyrrolidone (PVP) [64]. Additionally, natural, biomass and waste-derived sources of carbon can be used, such as shungite [65], bird droppings [66], wood [67], chicken manure [68], bamboo [69], cabbage [70], and beetroot [71]. However, these precursors also have traces of heteroatoms and metals, which may contribute to the overall enhanced activity. In heterogeneous catalysis, often, **non-carbon, Lewis acidic supports** are employed such as Al_2O_3 [72], CeO_2 [46], Nb_2O_5 [73], TiO_2 [74], and ZrO_2 [75]. Other supports, specifically, Mg$(OH)_2$ [76], MgO [77,78], SiO_2 [79,80], NaCl [64,81], and structure-directing polymers [82] are employed as **sacrificial supports**, which can later be removed by acid or base etching.

Crystalline porous materials, predominantly metal–organic frameworks (MOFs) and metal-modified covalent organic frameworks, are gaining recognition as promising carbon templates [83–85]. Since they are crystalline and have a precise topology, they give rise to carbonized materials that are highly ordered and are with high porosity, hence, have a large surface area. Typically, MOFs and metal-modified COFs have metals and heteroatoms already present, so no additional doping is required. In several examples, a metal exchange can be applied as a strategy to introduce new metals instead of the existing ones while maintaining the topology of the original MOF, e.g., by using zinc-based ZIF–8 as a precursor [86].

Doping with metals is typically done by pre-mixing the supports with metal salts or other metal-containing compounds before the carbonization step using ball milling, sonication, and thermal or hydrothermal treatments. The organometallic compounds used as co-dopants include metal porphyrins [87–89], metal phthalocyanines [90,91], or pre-formed metal complexes, for instance, with 1,10-phenanthroline [42,92].

In most cases, carbonization is carried out under inert gases (i.e., dinitrogen or argon). However, dihydrogen [51,93] or ammonia [94], which decomposes to give dihydrogen at higher temperatures, is often utilized to modify the atmosphere. This leads to an improved reduction of metal salts and oxides to give metal nanoparticles. The use of dioxygen, on the other hand, leads to the formation of metal oxides and/or partially oxidized carbon support, which may improve the overall conductivity and activity of the material.

Heteroatom doping is an essential modification in the fabrication of M–N–C materials because it leads to the formation of catalytic sites to which the metal can coordinate (Table 2). In addition to metal(0), metal oxides and metal carbides, heteroatoms also form other metal species,

Table 1
Most common sources for heteroatom doping.

heteroatom	heteroatom sources	ref
Boron	B(OH)$_3$	[109]
	B_2O_3	[110]
Phosphorous	phytic acid	[111,112]
	(NPCl$_2$)$_3$	[113]
	H_3PO_4	[114]
	NaH_2PO_2	[115]
Sulfur	KSCN	[116]
	S_8	[117]
	thioacetamide	[118]
	thiourea	[119]
Nitrogen	ammonia	[120]
	DABCO	[121]
	DCDA	[122]
	formamide	[123]
	melamine	[46]
	thiourea	[124]
	urea	[125]
	other	see Fig. 1
Oxygen	H_2O_2	[126]
	air	[127]
Fluorine	NH$_4$F	[128–130]
	HF	[131]
	PTFE	[132]

such as metal nitrides, sulfides, and phosphides. Finally, in some cases, heteroatom sites may act as catalysts without the necessity for a metal.

The nitrogen-ligated metal species (M–N_x, where x = 3–5) are the most widely studied ones [95]. Since doping with nitrogen is the most prevalent and the most critical contributor to the overall activity of M–N–C materials, a large number of nitrogen sources has been investigated to date (Table 1 and Fig. 1). When MOFs are used as precursors, nitrogen doping is not necessary because MOFs themselves have a high nitrogen content.

Chemical etching is performed with acids such as HF [95], HCl, HNO_3, H_2SO_4, or a combination thereof to remove metal oxides at the surface of catalyst materials. Sometimes base (e.g., NaOH [95]) can be used to remove silicon-based sacrificial supports. While electrocatalysts are always chemically etched, the materials used in heterogeneous catalysis are generally not etched. This, however, creates a misperception about the nature of catalytically active sites (e.g. nitrogen coordinated metal sites within the molecular network M–N_x) and other species (e.g., metallic and metal oxide nanoparticles). Often, chemically etched samples are subject to an additional carbonization step to remove nitro and sulfonyl groups formed during the acid treatment.

In addition to the primary synthetic strategies, such as those previously mentioned, it is essential to recognize the existence of various alternative methods for fabricating M–N–C catalysts. Notably, techniques like cage-encapsulation [96–98], gas-migration [99–102] and metalation [103–108] have gained prominence as significant approaches that enable precise control over the structural and performance characteristics of M–N–C catalysts. Moreover, there are several other noteworthy methods that contribute to the wide array of M–N–C catalysts, playing a pivotal role in tailoring their properties and reactivity. In the long term, there is a necessity for more well-thought-out fabrication methods to control better and fine-tune the properties of underlying catalyst materials. This is indeed needed, because there is a myriad of factors that contribute to the overall catalyst properties, including stability, activity, and, importantly, reproducibility.

The underlying catalyst material's nature and its catalytically active

Table 2
Optimization of reduction of nitrobenzenes.

Entry	Catalyst	GC yield, %	
		conditions A R = H	conditions B R = I
1	Fe(OAc)$_2$	0	<2
2	Fe(**L1**)$_x$	0	<2
3	Fe-**L1**/C-600	88	n.d.
4	***Fe-L1/C-800***	**98**	**94**
5	Fe-**L1**/C-1000	27	n.d.
6	Fe-**L2**/C-800	18	18
7	Fe-**L3**/C-800	30	44
8	Fe-**L4**/C-800	49	52
9	Fe-**L1**/Al$_2$O$_3$-800	78	n.d.
10	Fe-**L1**/TiO$_2$-800	49	n.d.

sites may vary drastically even if the same starting materials are used. Different active sites may arise from carbonization at various temperatures, acid etching with different acids, let alone in case if different supports are employed.

Metal nanoparticles and M–N$_x$ sites are the most commonly acknowledged active species. Characterization of active species gives a better insight into the mechanistic specifics of the processes involved. It provides a better understanding of the origin of the catalytic activity of the specific sites. Unfortunately, the acid etching step is often omitted when preparing the M–N–C materials used in heterogeneous catalysis. Indeed, this raises some questions about the nature of the active species involved. By merging the datasets obtained from several characterization techniques, one may better understand the composition and morphological changes between the active and spent catalysts. This information may further help us understand the catalytic processes and how to improve the catalyst's performance.

2. Applications in organic transformations

In this review, we emphasize the catalysts' preparation methods and their initial screenings. Often, a wide range of nitrogen precursors, supports and carbonization temperatures will be assessed to identify the best-performing catalyst for a particular class of transformations. Most of the reactions catalyzed by M–N–C materials are reductions and oxidations, which may be coupled with other processes such as aminations, condensations and esterifications. Most of the work reported to date has centered on using iron, cobalt and nickel catalysts. The authors often

named catalysts depending on the support, heteroatoms and carbonization temperatures used and may vary a lot.

2.1. Reduction of nitroarenes

2.1.1. Iron–based M–N–C catalysts for reduction of nitroarenes

Reduction of nitroarenes using M–N–C catalysts is the most extensively explored transformation [134,135]. In 2013, Jagadeesh et al. reported an iron-based M–N–C catalyst for the reduction of nitroarenes using dihydrogen at 50 bar (Table 2, conditions A) [34]. Several nitrogen-containing precursors (**L1**–**L4**) were screened using Vulcan XC72R as a carbon support. When carbonized at 800 °C, the Fe/phenanthroline (**L1**) system proved to be the most efficient (entries 4, 6–8). Notably, the reaction did not proceed using iron salt or non-carbonized iron–**L1** complex (entries 1 and 2). While carbonization temperature had to be optimized (entries 3–5), Al$_2$O$_3$ was not as efficient support as Vulcan XC72R (entry 9). Similar relationships between the precursors **L1**–**L4** and the yields were obtained for transfer hydrogenation of nitroarenes (Table 2; conditions B) [136].

Although none of the catalyst materials were acid etched, the total iron content in the sample and the amount of iron at the catalyst's surface were relatively low (2.95 wt% and 0.4 at%, respectively). Furthermore, the γ-Fe$_2$O$_3$ nanoparticles (2–5 nm and 20–80 nm) were surrounded by a protective graphitic carbon (3–5 layers). In the sample carbonized at 1000 °C the particles were larger and were not protected by the graphene layers. This indicates that γ-Fe$_2$O$_3$ nanoparticles, confirmed by Mössbauer spectroscopy, play a role in this heterogeneous process. The substrate scope for both transformations was particularly wide and included iodo, thio, cyano, formyl and alkynyl-containing substrates (Scheme 2).

By changing the carbon support from Vulcan XC72R to carbon nanotubes, Chen and co-workers achieved much lower catalyst loadings (0.33 mol% vs. 4.5 mol% Fe) [137]. However, over time, the species detected within the catalyst were oxidized from ε-Fe$_3$N to Fe$_3$O$_4$.

Renewable biomass can also be utilized to fabricate the M–N–C catalysts because it already contains all the heteroatoms needed and often gives rise to porous structures upon carbonization. In 2015, Shi et al. reported the synthesis of an active catalyst directly from biomass (glucose, sucrose, xylitol), which served as a carbon source (Table 3) [138]. A highly uniformed CNTs structure was obtained by mixing with FeCl$_3$, and melamine as a nitrogen source. The carbonization temperature significantly impacted the performance of a catalyst, with 700 °C being the optimal pyrolysis temperature (entry 3). Recycling tests showed ten rounds of stability without a significant drop in yield, and TEM micrographs revealed that the catalyst material remained unchanged. However, due to the fact that catalyst loading was initially higher than required during the stability test, a larger scale and longer duration of testing, for example, a continuous flow test, is needed to confirm the stability of M–N–C materials [139]. The catalyst was used for reduction of nitroarenes and alkenes with excellent functional group compatibility (Scheme 3).

Other biomass-derived systems, such as chitosan [140] and bamboo [141] can also be used to fabricate mesoporous carbon, albeit doping with iron salts is needed. Depending on different carbonization temperatures and co-dopants, these contained various iron species (Fe$_3$O$_4$, FeN$_x$, FeC$_x$ and FeS$_2$) and were utilized for the reduction of nitroarenes. Also, MOFs such as spindle-shaped Fe-MIL-88A can simultaneously be
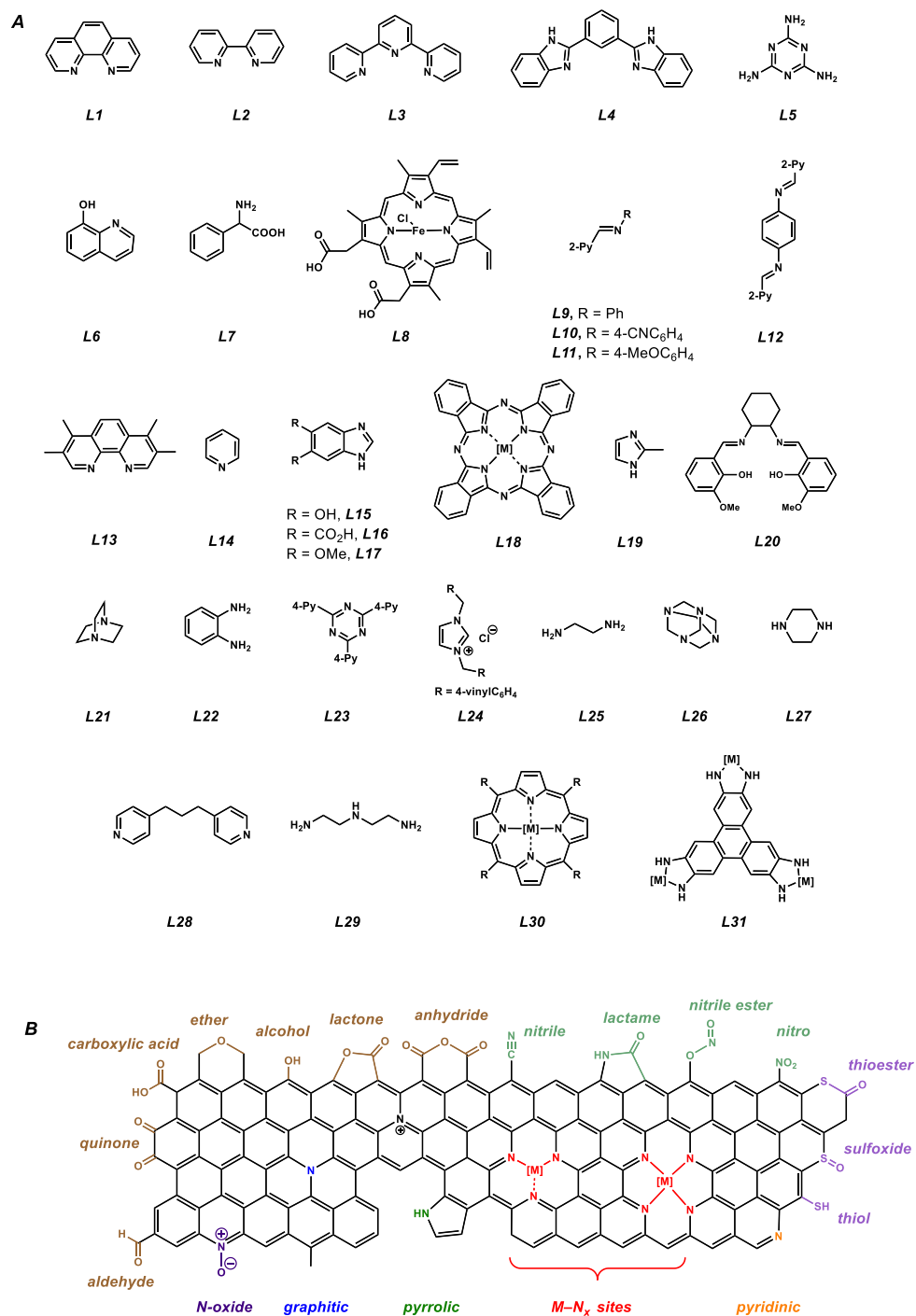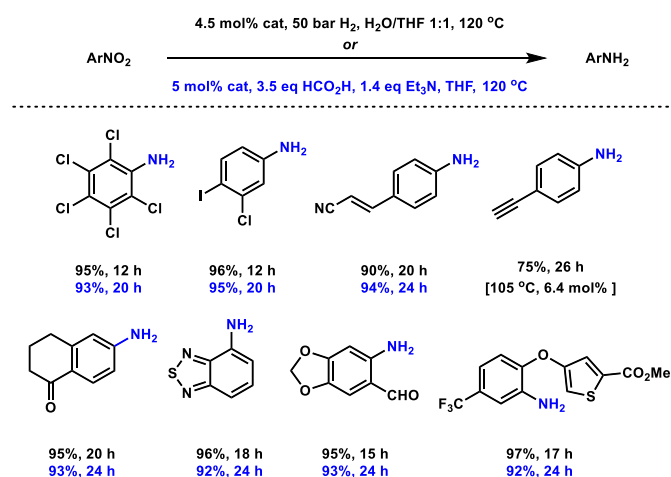
Fig. 1. (A) Widely used nitrogen-containing precursors for M–N–C catalysts. (B) Different heteroatom based catalytic species [133].

Scheme 2. Reduction of nitroarenes with dihydrogen (black) and formic acid (blue).

used as a support and nitrogen source [142].

Li and co-workers screened a large subset of Fe–N–C catalysts to find an optimal M–N–C catalyst for the reduction of furfural to furfuryl alcohol under transfer hydrogenation conditions (Table 4) [36]. They employed activated carbon (AC) as support, as Lewis acidic supports (SiO$_2$, Al$_2$O$_3$, TiO$_2$) were not so effective (entries 1, 10–12). Out of six precursors, 1,10-phenanthroline (**L1**) outperformed the rest, which was 2,2′-bipyridine (**L2**), 2,2′:6′,2″-terpyridine (**L3**), 8-hydroxyquinoline (**L7**), phenylglycine (**L8**) and hemin (**L9**) (entries 1, 3–7). Using cobalt or nickel in place of iron did not improve the activity (entries 8 and 9), however, conducting the reaction in 2-butanol did improve all the parameters, and the final system was on par with 5 wt% Ru/C. During the recycling tests, iron leaching was minimal (<1%), suggesting that Fe–N$_x$ sites and α–Fe drive the reduction process. Indeed, the spent catalyst had fewer Fe–N$_x$ sites (as measured by XPS) and PXRD detected the formation of Fe$_2$O$_3$.

Sahooo et al. have introduced Schiff bases as modular precursor and used them for the reduction of quinolines and another heteroarene (Scheme 4) [35]. They found that the precursor (**L12**) prepared by condensation of 2-pyridinecarboxaldehyde and para-phenylenediamine led to significantly better conversions. Vulcan XC72R served as a better support than SiO$_2$, Al$_2$O$_3$ and TiO$_2$. Solvent, imine loading and carbonization temperatures were also optimized.

The active catalyst contained Fe$_3$C nanocrystals surrounded by N-doped graphene layers. Although the reduction reactions were slow (up to 72 h), the catalyst was active for at least seven runs when quinaldine was used as substrate. While no significant iron leaching into the solvent

Table 3
Optimization of hydrogenation of nitrobenzene.

Entry	Catalyst	Conv, %	Selectivity, %
1	Fe$_3$C@G-CNT-600	58.6	91.5
2	Fe$_3$C@G-CNT-650	84.1	91.5
3	Fe$_3$C@G-CNT-700	100.0	98.3
4	Fe$_3$C@G-CNT-750	92.4	91.1
5	Fe$_3$C@G-CNT-800	79.5	90.8
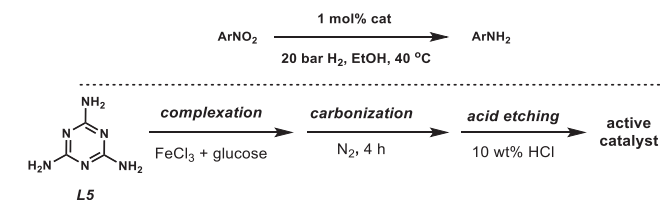
had been observed, the spent catalyst had Fe$_3$O$_4$, as confirmed by PXRD. Acid etching of the catalyst did not improve the conversions.

2.1.2. Cobalt–based M–N–C catalysts for reduction of nitroarenes

In 2013, Westerhaus et al. profiled several nitrogen-rich precursors in combination with cobalt (Table 5) [41]. The same precursors were previously used to fabricate iron catalysts [34]. In both cases, 1,10-phenanthroline showed the best activity, and Co–N–C material outperformed the Fe–N–C analog. The most active catalyst had NPs size predominantly 2–10 nm, with some larger agglomerates (up to 800 nm), while the less efficient catalyst based on 2,2′:6′,2″-terpyridine (**L3**) had a narrower distribution of nanoparticles. The Co–N–C catalyst was used for the reduction of a wide range of substrates, including alkynes, heterocycles, iodides and aldehydes (Scheme 5). It was recycled ten times with little loss in yield if the reaction was run for 12 h. Interestingly, the reaction was faster when water was used as a solvent, hinting at the ʼon water effect [143].
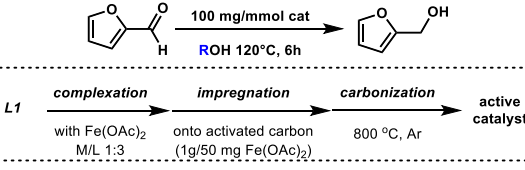
In 2015, Wei et al. prepared metallic Co and Co$_3$O$_4$ nanoparticles containing material from a combination of melamine, D-glucosamine and cobalt nitrate (Scheme 6) [144]. Importantly, under these conditions, the carbon network was transformed into nitrogen- and metal-decorated carbon nanotubes. The carbonization temperature was optimized, and many functional groups were tolerated.

Zhou et al. prepared a Co–N–C catalyst by using cobalt phthalocyanine as a source of both metal and nitrogen, and SiO$_2$ was used as a sacrificial support (Table 6) [95]. SiO$_2$ was later removed by treating the carbonized sample with either HF or NaOH. Acid-treated (AT) catalysts contained only Co–N$_x$ sites, whereas base-treated (BT) ones contained metallic cobalt NPs. It was shown that the active Co–N$_x$ species were formed at 800 °C but decomposed at higher temperatures. Hydrogenation and transfer hydrogenation of nitroarenes were performed in water and showed high functional group tolerability. Furthermore, nitroalkanes were successfully reduced to primary amines. The catalyst remained active for eight rounds, and no metal leaching was observed.

Crystalline MOFs, which contain nitrogen ligands (most commonly, 2-methylimizadole), can give rise to M–N–C materials. Their shape and topology can be controlled, which can lead to highly organized, porous materials. Using hexadecyltrimethylammonium bromide (CTAB) as a surfactant, Yang et al. prepared nano box-shaped ZIF-67 (Scheme 7). It was then treated with red phosphorous [118] or thioacetamide [145] to introduce phosphorous or sulfur, respectively, and were subjected to pyrolysis to give materials that contained either Co$_2$P or Co$_3$S$_4$ nanoparticles. In addition, they also contained Co–N$_x$ sites. Both catalysts were tested to reduce nitroarenes with H$_2$, showed excellent scope and were stable in the recycling tests. The authors suggest that NPs are the main reactive species, which was not sufficiently demonstrated. A similar N, S-co-doped catalyst was obtained from porous organic polymers [146].

Yuan et al. profiled a series of Co–N–C heterogenous catalysts prepared from sucrose and melamine for transfer hydrogenation with formic acid (Table 7) [147]. The authors demonstrate that the carbonization temperatures had a significant impact on catalysts's performance, with the activity order being 600 > 700 > 800 > 500 > 400 °C (entries 1–5). Among the iron triad metals, Co was the best one (entries 1, 6, 7). Interestingly, the cobalt salt also had a role to play in the

Scheme 3. Substrate scope for reduction of nitroarenes.

Table 4
Optimization of transfer hydrogenation of furfural to furfuryl alcohol.

Entry	Catalyst	Conv., %	Yield, %	Selectivity, %
1	Fe-**L1**/AC-800	51.5	44.0	85.4
2[a]	**Fe-L1/AC-800**	**71.3**	**60.0**	**84.2**
3	Fe-**L2**/AC-800	26.4	15.2	57.6
4	Fe-**L3**/AC-800	40.3	34.0	84.4
5	Fe-**L7**/AC-800	21.3	10.8	50.7
6	Fe-**L8**/AC-800	5.2	3.7	71.2
7[b]	**L9**/AC-800	49.2	41.3	83.9
8	Co-**L1**/AC-800	17.1	5.4	31.6
9	Ni-**L1**/AC-800	13.5	5.5	40.7
10	Fe-**L1**/SiO$_2$-800	32.8	16.3	49.7
11	Fe-**L1**/Al$_2$O$_3$-800	18.0	4.3	23.9
12	Fe-**L1**/TiO$_2$-800	32.8	13.7	41.8
13[c]	Ru/C	96.9	59.9	61.8

[a] *i*-BuOH as a solvent.
[b] **L9** incorporates iron metal.
[c] Metal loading: 5 wt%.

Scheme 4. Hydrogenation of N-heterocycles.

final catalyst activity (acetate > nitrate > chloride) (entries 1, 8, 9). Moreover, metallic cobalt supported on activated carbon showed good yield for the first round. However, the catalyst was uuterly not active after recycling. This suggests that entrapment by Co NPs into nitrogen-

doped carbon support is necessary for the longevity of the catalyst. The Co@NC-600 catalyst with an average NP size of 10.3 nm was recycled for five rounds without loss in yield. While no morphological changes were observed, the magnetism of the catalyst slightly dropped from 14.09 emu/g to 12.7 emu/g.

Catalysts for nitroarene reduction were also prepared from biomass (Scheme 8). Sahoo *et al.* used chitosan, a nitrogen-containing biopolymer from crab and shrimp shells, to gain access to a material that contained metallic Co and Co$_3$O$_4$ NPs and Co–N$_x$ sites embedded into the carbon matrix [148]. For efficient reduction of nitroarenes, this material required the addition of triethylamine as a base. Duan *et al.* demonstrated that fresh bamboo shoots can also be used for the fabrication of cobalt-based active catalysts [149]. However, additional doping with phosphorous in the form of triphenylphosphine was needed for transfer hydrogenation with ammonium formate.

Liu *et al.* reported Co–N–C material, the synthesis of which was optimized to ensure a higher percentage of single atom sites without any presence of Co or Co$_3$O$_4$ NPs [42]. It was achieved by impregnating Mg(OH)$_2$ support with cobalt phenanthroline complex, followed by carbonization at 700 °C and subsequent acid etching with nitric acid. The material was then used for the partial reduction of nitroarenes to azo compounds, whereas the addition of sodium hydroxide was crucial (Scheme 9). The catalyst could be recycled, provided that the reaction time was prolonged.

Schwob *et al.* developed a Co–N–C catalyst based on a salen complex and used it to prepare 1*H*-pyrimidine from 1,8-dinitronaphthalene and an aldehyde (Scheme 10) [150]. During catalyst preparation, the carbonized material was reduced in a mixture of N$_2$ and H$_2$ to ensure that only metallic cobalt (not oxides) nanoparticles with a mean diameter of 7 nm get entrapped by carbon shells. Activated charcoal was used as support. Metal oxides (TiO$_2$, CeO$_2$, γ-Al$_2$O$_3$) were less effective and led to the reduction of an aldehyde. Various sensitive moieties, including iodo, alkynyl and boronate, were compatible with the reaction conditions.
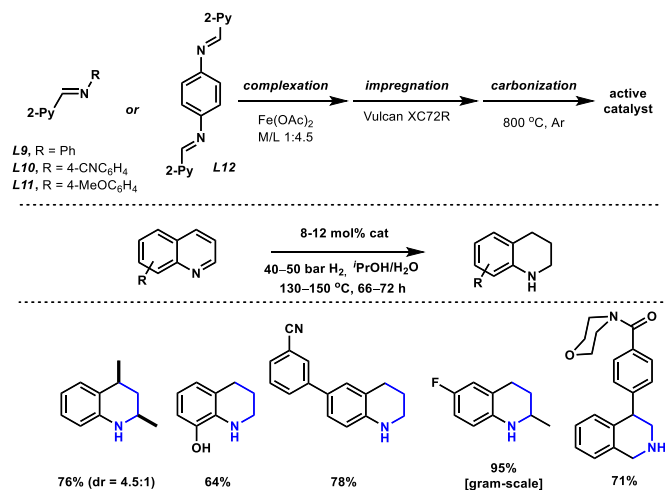
2.2. Hydrogenation of heterocycles and unsaturated hydrocarbons

For the reduction of quinolines and indoles, Chen *et al.* reported a catalyst based on 1,10-phenanthroline as precursor and α-Al$_2$O$_3$ as support (Table 8) [45]. Interestingly, when iron was used as the metal source while keeping the rest components the same, the resulted catalyst was much less efficient. HAADF and EDX also revealed that the NPs had a core–shell structure with Co$_3$O$_4$ being outside (3 nm) and metallic Co being inside (20 nm). The catalyst was recycled for six runs, and ICP–MS did not detect metal leaching. However, the yield decreased continuously. These results demonstrate that dispersed metallic cobalt nanoparticles are responsible for the catalytic properties.

A different cobalt-based catalyst based on melamine as a nitrogen source was used to fully reduce pyridines. A wider set of Lewis acidic supports was tested (CeO$_2$, ZrO$_2$, Nb$_2$O$_5$, BN, carbon, Al$_2$O$_3$) and TiO$_2$ came out on top (Scheme 11) [46]. With formic acid as a hydrogen donor, a similar catalyst supported on Vulcan XC72R was used [151].

Other organic precursors used for similar transformation include a combination of melamine and glucosamine [152] and ethylenediamine [153].
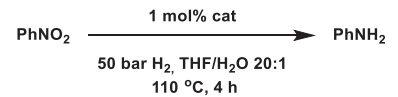
Co–N–C materials can catalyse the reduction of unsaturated hydrocarbons. Chen *et al.* developed a catalyst based on 1,10-phenanthroline and silica support for selective hydrogenation of alkynes to alkenes (Table 9) [47]. Other supports such as activated carbon, aluminum

Table 5
Optimization of reduction of nitrobenzene.

Entry	Precursor	Conv., (yield),[a] %
1	Co-**L1**	4(0)
2	Co-**L1**/NC	>99(95)
3	Co-**L2**/NC	8(5)
4	Co-**L3**/NC	26(19)
5	Co-**L4**/NC	<1(0)
6	Co-**L15**/NC	<1(0)
7[b]	Fe-**L1**/NC	15(1)

[a] Determined by GC analysis using n-hexadecane as the internal standard.
[b] Reaction time 16 h.
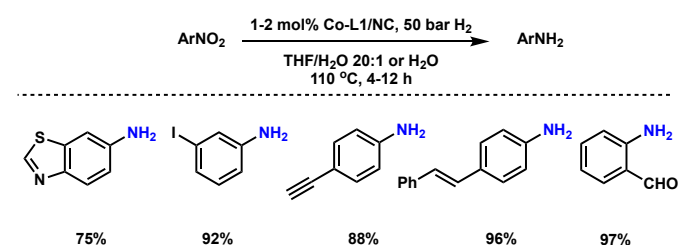
Scheme 5. Substrate scope for reduction of nitroarenes. Yield was determined by GC analysis using n-hexadecane as the internal standard.
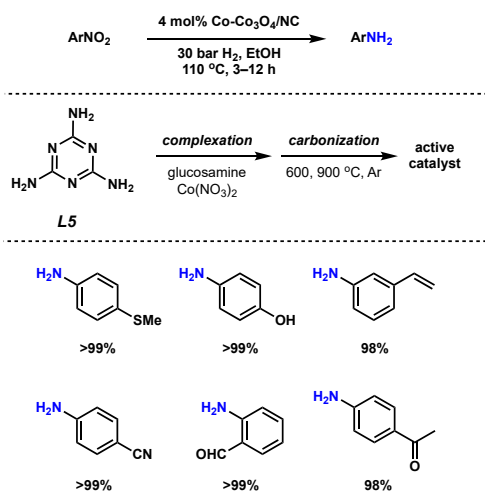
Scheme 6. Substrate scope for reduction of nitroarenes.

oxide and boron carbide resulted in poorer conversions and selectivities (entries 1–3). The active catalyst contained metallic cobalt, CoO and Co_3O_4 surrounded by N-doped graphitic layers. Acid leaching of the initial material with HCl washed away cobalt oxides from the catalyst's surface; hence, it reduced activity and selectivity. Catalyst optimally carbonized at 800 °C can be used in the selective reduction of both terminal and internal alkynes with high selectivity for *cis*-alkene (Scheme 12).

Liu *et al.* succeeded in complete reducing phenols typically extracted from lignin valorization to the corresponding alkanes via a

hydrodeoxygenation reaction (Scheme 13) [120]. The Co–N–C catalyst was fabricated from cellulose and nitrogen was introduced in the form of ammonia. From XRD patterns, the authors conclude that the catalyst contains cobalt nitride as the active species. On recycling, the catalyst gradually loses its activity and might require regeneration.

Chitosan-derived catalyst was developed by Scharnagl and co-workers and was used for the hydrogenation of alkenes (Scheme 14) [154]. The catalyst contained metallic Co nanoparticles as major species and were coated with N-doped graphitic carbon. It was recycled for nine runs without a drop in activity or metal leaching. However, the formation of cobalt oxides was observed after stability tests. A great number of functional groups were tolerated, including alcohols, epoxides, imidazolyl, halides, anilines and tertiary amines.

2.3. Reductive amination

In 2017, Jagadeesh *et al.* reported (terephthalic acid) TPA and DABCO based *in situ* MOF-derived cobalt catalyst for reductive amination (Scheme 15) [121]. The authors screened various metals and carbonization temperatures. Still, they did not treat the pyrolyzed material with acid, so additional metal or metal oxide nanoparticles might have been present at the surface. Using Vulcan XC72R as carbon support, iron, copper and manganese-based catalysts were completely inactive, while nickel showed limited activity. The active catalyst contained majorly metallic Co NPs (5–30 nm) surrounded by the graphitic layers. A smaller number of core–shell particles with Co_3O_4 shell at the metallic cobalt were also detected. Both ketones and aldehydes were used, and it was possible to use nitroarenes in place of amines. A similar catalyst system was applied to transfer hydrogenation of other substrates such as nitroarenes, nitriles, aldehydes and ketones [155,156].

ortho-Phenylenediamine was reported as a precursor to M–N–C material by Yuan *et al.* (Scheme 16) [157]. They used SiO_2 as support, and the initial cobalt–phenylenediamine complex was allowed to polymerize using H_2O_2, and the catalyst was acid etched with HF before use. The catalyst contained metallic cobalt nanoparticles with a mean size of 13 nm, and the optimal solvent was ethanol. Both aromatic and aliphatic aldehydes could be used as substrates. Interestingly, from the kinetic studies, the authors found that amination does not only proceed by hydrogenation of the imine formed from aldehyde and ammonia. Instead, the final amine reacts with an aldehyde to give an intermediatory Schiff base, which is then transformed by ammonia into aminal and subsequently is hydrogenated. Overall, the reported Co–N–C catalysts outperformed several other systems based on precious metals (Pt-MoO_x-TiO_2, Ru/Nb_2O_5 and Ru NP).

Other cobalt systems for reductive amination use formic acid as a hydrogen donor and employ catalysts previously discussed above for differenr applications (phthalocyanine [43,95] and phenanthroline [41,158] as precursors).
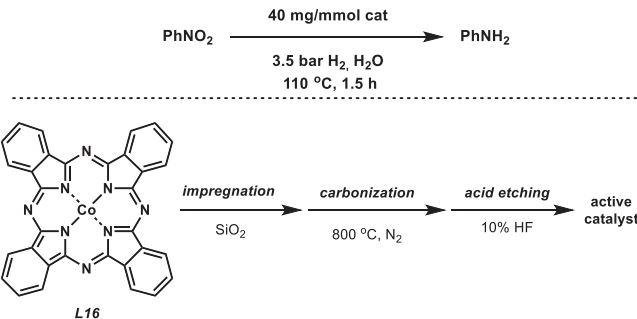
2.4. Oxidative transformations

2.4.1. Fe-N-C catalysts for oxidative transformations

Iron is one of the key elements involved in biologically relevant oxidative processes; hence, a substantial amount of work done with Fe–N–C materials centered on oxidation reactions [159,160].

Jagadeesh *et al.* used previously reported catalyst [34] based on 1,10-phenanthroline (**L1**) to catalyze the oxidation of primary amines to the corresponding nitriles (Scheme 17) [38]. Similarly to the previous case [34], other organic precursors such as 2,2′-bipyridine (**L2**), 2,2′:6′,2″-terpyridine (**L3**) and 2,6-bis(2-benzimidazolyl)pyridine (**L4**) gave rise to much less effective catalysts.

Beller et al. have also described an iron-zeolite derived catalyst Fe_1-N-C for the transformation of selective ammoxidation of alcohols to nitriles [161], the catalytic sites was characterized to be Fe–N_4 moieties, while the catalytic activity of the nanoparticle based catalyst Fe_2O_3-NGr/C was tested to be much lower. Same transformation was also
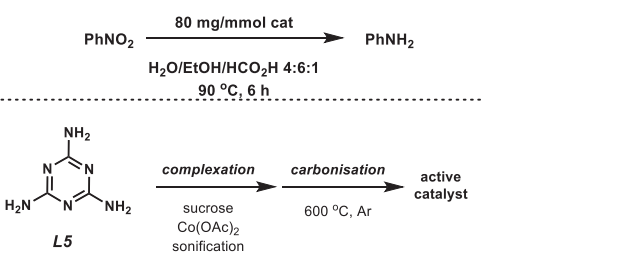
Table 6
Optimization of reduction of nitrobenzene.

$$PhNO_2 \xrightarrow[\substack{3.5 \text{ bar } H_2, H_2O \\ 110\ ^{\circ}C, 1.5\ h}]{40 \text{ mg/mmol cat}} PhNH_2$$

L16

$$\text{L16} \xrightarrow[SiO_2]{impregnation} \xrightarrow[800\ ^{\circ}C, N_2]{carbonization} \xrightarrow[10\% \ HF]{acid\ etching} \text{active catalyst}$$

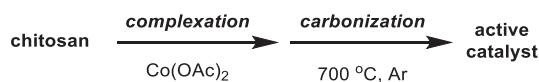| Entry	Catalyst	Conv.,%
1	Co-L16	0
2	Co-LX/NC-400-AT	0
3	Co-LX/NC-600-AT	9.0
4	Co-LX/NC-800-AT	100.0
5	Co-LX/NC-900-AT	70.8
6[a]	Co-LX/NC-800-AT	47.1
7[a]	Co-LX/NC-800-BT	54.0

[a] Reaction time 0.5 h.
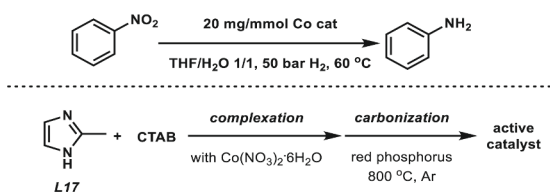
Scheme 7. Preparation of Co_2P and Co_3S_4 nanoparticle-containing catalysts.

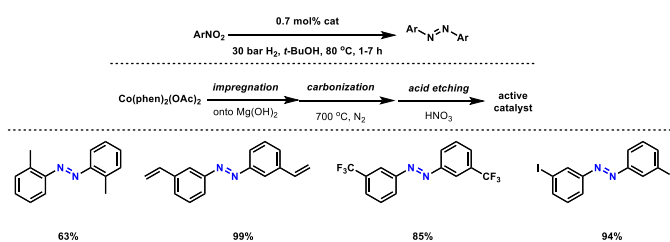**Table 7**
Optimization of reduction of nitrobenzene.

$$PhNO_2 \xrightarrow[\substack{H_2O/EtOH/HCO_2H\ 4:6:1 \\ 90\ ^{\circ}C, 6\ h}]{80 \text{ mg/mmol cat}} PhNH_2$$

Entry	Catalyst	Metal sourse	Yield,[a] %
1	Co@NC-400	Co(OAc)$_2$	1.7
2	Co@NC-500	Co(OAc)$_2$	13.3
3	Co@NC-600	Co(OAc)$_2$	99.9
4	Co@NC-700	Co(OAc)$_2$	32.4
5	Co@NC-800	Co(OAc)$_2$	24.6
6	Fe@NC-600	Fe(acac)$_2$	7.8
7	Ni@NC-600	Ni(acac)$_2$	3.6
8	Co@NC-600*	CoCl$_2$	18.0
9	Co@NC-600*	Co(NO$_3$)$_2$	68.9

[a] Determined by GC–MS.

$$\text{chitosan} \xrightarrow[Co(OAc)_2]{complexation} \xrightarrow[700\ ^{\circ}C, Ar]{carbonization} \text{active catalyst}$$
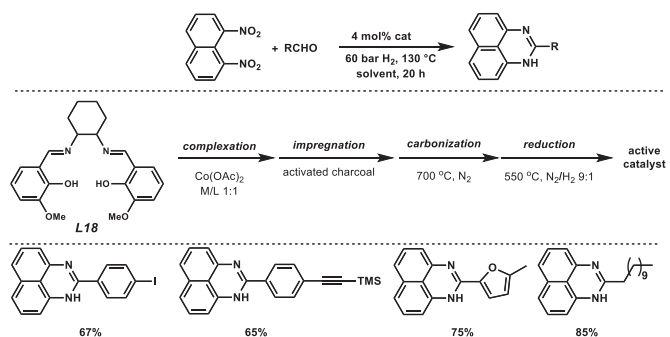
Scheme 8. Preparation of chitosan derived catalysts.

Scheme 9. Substrate scope for partial reduction of nitroarenes to azo compounds.

Scheme 10. Reduction of aldehydes with 1,8-dinitronaphthalene using Co–N–C catalyst derived from a salen complex.

reported with a catalyst based on cobalt [162].

In 2015, Cui and co-workers prepared an iron-based nanocatalyst, which was quite similar to the one employed earlier [34,38] and used it for oxidative dehydrogenation of *N*-heterocycles (Scheme 18) [37]. The difference was the material was acid-leached with 5 M HCl overnight. This was done to remove agglomerated nanoparticles from materials surface, leaving graphite-protected iron oxide nanoparticles, which improved conversions. Additionally, 3,4,7,8-tetramethyl-1,10-phenanthroline (**L13**) and pyridine (**L14**) were screened as potential precursors; however, they did not lead to improvements. This transformation has also been reported by Stahl in 2015 with a heterogeneous cobalt oxide catalyst [163].

In 2017, Zhang *et al.* profiled a series of heterogenous iron catalysts based on phenanthroline precursors (Scheme 19) [39]. Importantly, MgO was used as a sacrificial template to ensure well distributed Fe–N$_x$ sites within the material and to prevent the formation of the iron-based nanoparticles. The catalyst was also acid leached to expose single-atom sites. Out of the three different carbonization temperatures, a material carbonized at 700 °C was the best-performing one. The active catalyst contained single atom Fe–N$_x$ sites, while no α–Fe or iron oxides were detected. Mössbauer spectroscopy provided more detailed information, suggesting that more Fe–N$_5$ species in the Fe–N–C–700, which was confirmed by kinetic studies using poisoning of a catalyst with potassium thiocyanate. Mechanistically, the oxidation of ethylbenzene was shown to undergo a radical pathway. Aerobic oxidation of alcohols was described by Davis et al. in 2016 on the iron-based heterogeneous catalyst, while the activity of the catalyst needs to be fully regenerated upon treatment of the used catalyst with H$_2$ [164]. Several recent studies unveil the relationship between M–N–C catalysed thermochemical and electrochemical oxygen reduction reaction [165–167]. Stahl and Root proved that unlike electrochemical ORR and noble-metal catalysed aerobic oxidation, which proceeded through coupling of two independent half-reactions (IHR), hydroquinone-mediated oxygen reduction with M–N–C catalysts involved a direct inner-sphere reaction (ISR) mechanism [166]. In addition to the ISR mechanism, Stahl and Surendranath also proposed a band mediated pathway of metals instead of sequential redox cycling pathways of molecules. By carrying out

Table 8
Optimization of hydrogenation of quinoline.

Entry	Catalyst	H_2, bar	Yield,[a] %
1	Co/L1/α-Al$_2$O$_3$	10	90
2	Co/L2/α-Al$_2$O$_3$	10	37
3	Co/L3/α-Al$_2$O$_3$	10	52
8	Co/L1/α-Al$_2$O$_3$	20	98
9	Co/L1/SiO$_2$	20	93
10	Co/L1/MgO	20	35
11	Co/L1/B$_4$C	20	34
12	Fe/L1/α-Al$_2$O$_3$	20	<5

[a] Determined by GC analysis using dodecane as the internal standard.
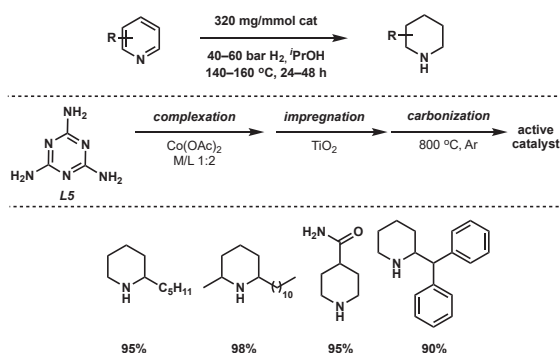
Scheme 11. Substrate scope for reduction of N-heteroarenes.

operando study and selective poisoning experiments, oxygen reduction was proved to proceed at cobalt sites, while hydroquinone oxidation happened at carbon-oxide defects [165], and this study also provides insights into catalyst deactivation pathways. Another report by Surendranath provided a link between thermochemical and electrochemical catalysis, and showed that in aerobic thermochemical oxidations,

Table 9
Optimization of hydrogenation of 1,2-diphenylethyne.

Entry	Catalyst	Conv.,[a] %	Regioselectivity, Z/E
1	Co/L1@C-800	68	58:9
2	Co/L1@α-Al$_2$O$_3$-800	16	3:13
3	Co/L1@B$_4$C-800	100	74:26
4	Co/L1@SiO$_2$-600	76	70:6
5	Co/L1@SiO$_2$-700	99	78:21
6	Co/L1@SiO$_2$-800	100	90:9
7	Co/L1@SiO$_2$-900	99	90:10
8	Co/L2@SiO$_2$-800	62	58:4
9	Co/L3@SiO$_2$-800	99	88:10

[a] Determined by GC analysis.
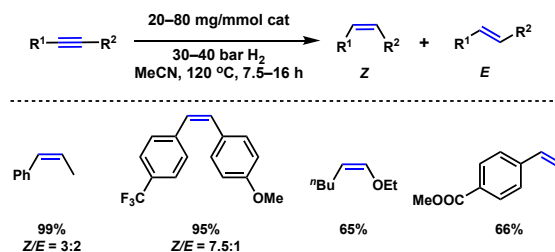
Scheme 12. Substrate scope for hydrogenation of alkynes.

oxygen, as an electron scavenger, supplied electrochemical driving force for organic substrate oxidation [167].

While most reports to date profile catalysts derived from 1,10-phenanthroline, Ping and co-workers reported a series of new catalysts based on the 5,6-disubstituted benzoimidazole framework (Scheme 20) [168,169]. The active catalyst contained Fe/Fe$_3$C nanocrystals and Fe–N$_x$ sites, which can also be used in electrocatalysis for oxygen reduction and evolution reactions [169]. Interestingly, methylarenes are oxidized to give carboxylic acids.

Uncarbonized catalysts showed no effect on the oxidation of toluene, and it caused fast decomposition of TBHP, probably due to the high metal content. Catalyst **C10** can be used to transform polymethylated arenes (m-xylene/mesitylene) into diacids with a reasonable yield, avoiding toxic reagents, for example, KMnO$_4$. The recycling test showed three rounds of full conversion.

Song *et al.* profiled a series of heterogenous iron catalysts based on bamboo shoot-derived carbon and nitrogen support with additional PPh$_3$ as a phosphor source for oxidative transformations of alkenes (Table 10) [40]. Doping with phosphorous was essential for better selectivities (entries 1–4). Out of the three different carbonization temperatures, 800 °C was optimal for the best-performing catalyst (entry 2) with the smallest size of Fe/FeC$_x$ nanoparticles (3.6 ± 0.9 nm). XPS revealed the presence of Fe–N$_x$ and FePO$_4$ sites in the catalyst, the latter contributing to the overall reaction progress as Lewis acidic sites. The pyridine poisoning experiment confirmed the necessity of FePO$_4$ species.

These catalysts were used to selectively convert alkenes to ketones *via* Meinwald rearrangement or diketones via nucleophilic ring-opening of the intermediate epoxide (Scheme 21). For ring-opening to be the preferred pathway, the addition of *tert*-butylammonium iodide was required.

In 2021, Song *et al.* reported another application of Fe@NPC–800 in preparation of α-diketones [170]. Namely, diketones were obtained from aldehydes and methylketones *via* oxidation of an intermediatory aldol condensation products. Unlike previous examples, this was achieved using H$_2$O$_2$, not TBHP, as a terminal oxidant. The initial condensation step gave α,β-unsaturated ketones followed by epoxidation and
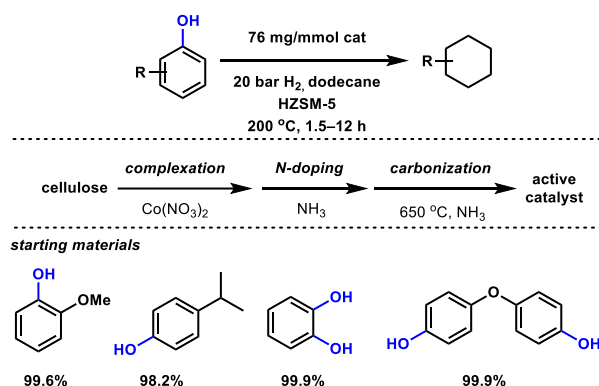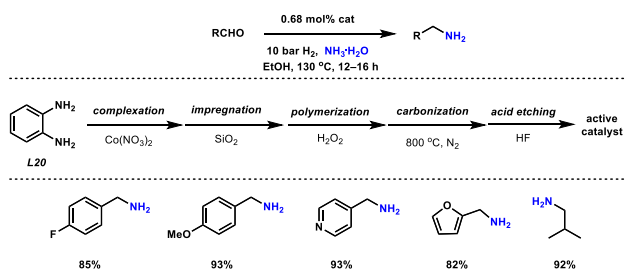

Scheme 13. Substrate scope for complete reduction of phenols.
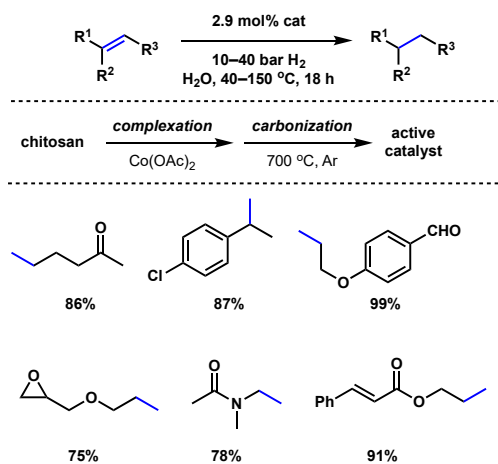
Scheme 14. Substrate scope for reduction of alkenes.
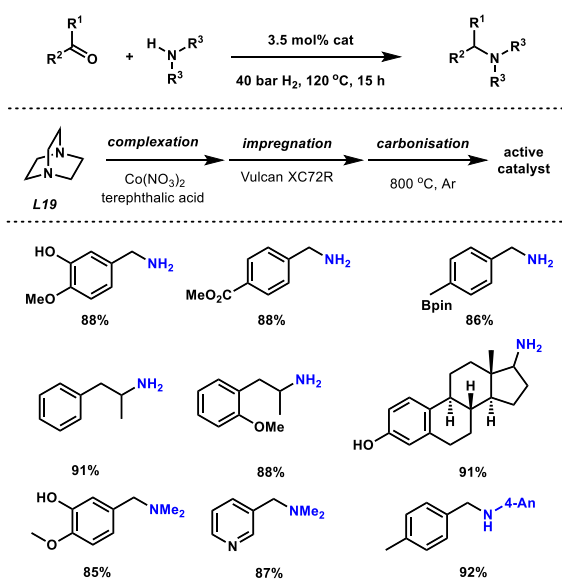
Scheme 15. Reductive amination of aldehydes and ketones using Co–N–C catalyst derived from MOF.

Scheme 16. Reductive amination of aldehydes using Co–N–C catalyst derived from o-phenylenediamine.

the Meinwald rearrangement to yield a one-carbon skipped diketones (Scheme 22). The underlying catalyst could be recycled for at least six rounds without any significant drop in the yield, and a wide range of aldehydes and ketones were efficiently utilized.

2.4.2. Co-N-C catalysts for oxidative transformations

Oxidation is a major class of reactions in which Co–N–C catalysts are often utilized. Most such transformations center on oxidative esterifications, where primary or secondary alcohols are converted into the corresponding esters.

In 2013, Jagadeesh and co-workers screened several standard precursors to identify that once more, the 1,10-phenanthroline/Vulcan XC72R system obtained by carbonization at 800 °C was the optimal cobalt oxides-containing catalyst (Table 11, entry 5) [171]. Various combinations of alcohols were exemplified (Scheme 23).

Su *et al.* screened a series of cobalt catalysts derived from a mixture of $Co(NO_3)_2$, 1,4-benzenedicarboxylic acid, DABCO, and various amounts of graphitic carbon nitride (g-C_3N_4) as carbon support for oxidative esterifications [62]. The authors demonstrated that variating the g-C_3N_4 ratio to the other components affected catalysts' performances due to the electron flow from metallic cobalt nanoparticles to the support, also referred to as the Mott–Schottky effect [172].

Another catalytic system, that relied on the carbonization of a cobalt-containing MOF (ZIF-67), was developed for oxidative esterification at room temperature [49]. Metallic cobalt nanoparticles surrounded by graphitic carbon were reported as catalytic species, and this was verified by deactivating the catalyst with aqua regia (48 h) to remove Co NPs. Several additional examples of lactonization of diols were reported.

Carbonization of the same MOF at a lower temperature and for a shorter period gave rise to a mixed Co oxide/Co(0) containing Co–N–C material, which required higher reaction temperatures and the addition of K_2CO_3 to drive ester formation [173]. If no oxygen was present, the alcohol was converted to the corresponding aldehyde.

Xie *et al.* used zirconium and 2-aminoterephthalic acid-derived MOF UiO-66-NH$_2$ as a template, into which cobalt and DABCO were introduced (Scheme 24). After pyrolysis at 800 °C, the material contained Co-N_x sites in a zirconium oxide/N-doped carbon matrix [174]. In the presence of *p*-nitrobenzoic acid (PNBA), this catalyst prepared a variety of quinazolinones.

One way to gain access to materials with highly dispersed Co–N_x sites is to carbonize bimetallic zinc and cobalt-containing MOFs because of zinc boiling temperature (bp = 907 °C) [175]. Nie *et al.* used such materials to induce aerobic oxidation of alkylarenes utilizing a combination of O_2 and TBHP. Typically, complex mixtures of products (alcohols,
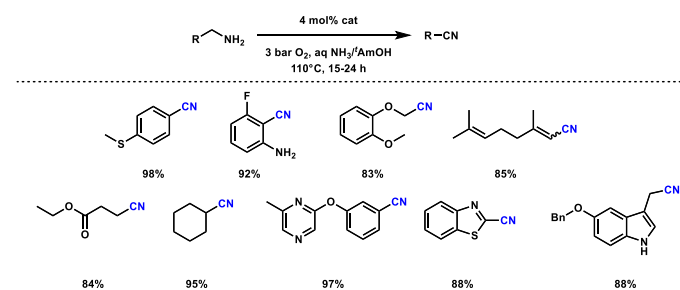
Scheme 17. Dehydrogenation of primary amines to nitriles.
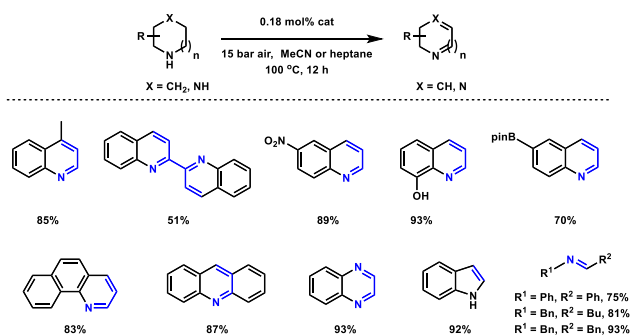
**Scheme 18.** Dehydrogenation of N-heterocycles.
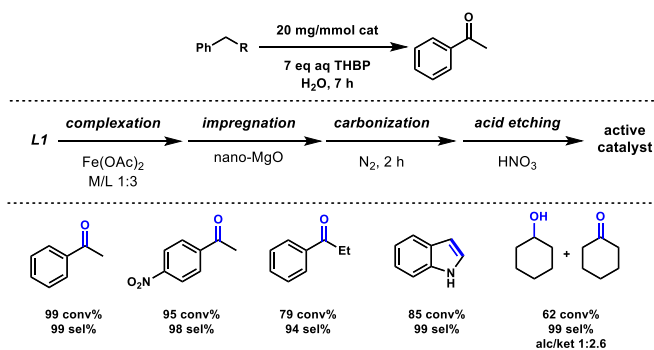
Scheme 19. Oxidation reactions using the acid etched catalyst.

aldehydes or ketones, carboxylic acids) were obtained [51].

Using silica as a sacrificial support often allows the creation of pores where nanoparticles can grow. Luo and co-workers used this strategy to prepare a catalyst that was able to cleave carbon–carbon bonds in activated alcohols to give corresponding esters (Scheme 25) [48].

Recently, Ping et al. reported a cobalt catalyst derived from an amorphous cobalt MOF, which was based on a carbon-rich benzimidazole precursors [169]. This allowed simpler conditions to obtain Co–N–C materials with metallic cobalt nanoparticles (Scheme 26) [176]. Alkylarenes were shown to be oxidized either to ketones or carboxylic acids with TBHP as the terminal oxidant. The addition of acetic acid improved the yields in case of oxidation of methylarenes carboxylic acids while adding a base deactivated the system. Carbonization temperatures significantly impacted the performance and stability of the catalyst during oxidation reactions. The active catalyst was used for up to six rounds without loss in yield for the oxidation of toluene and diphenylmethane.
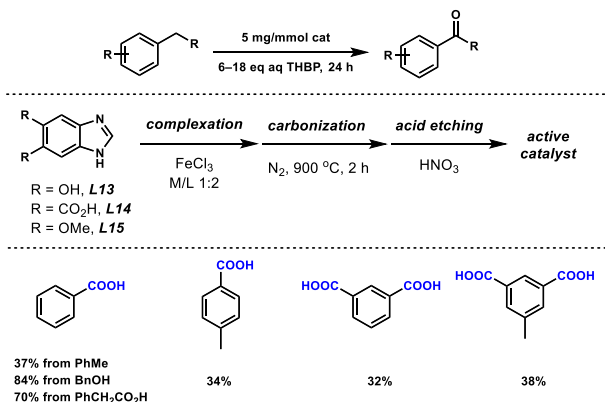
Scheme 20. Substrate scope for oxidation of C–H bond.

A triazine precursor was introduced as a nitrogen source by Bai et al. They utilized triazine to prepare a catalyst, which in the presence of TBHP, induced oxidative amidation of aldehydes with N-formamides (Scheme 27) [52]. Metallic cobalt nanoparticles entrapped into N-doped carbon assisted in this radical reaction. A similar catalyst carbonized at 700 °C was employed for the aerobic oxidation of alcohols to aldehydes and ketones [177]. Alternatively, Zn/Co yolk–shell catalyst can be used for this transformation [50].

2.5. Miscellaneous

Sarkar and co-workers recently demonstrated applying the 1,10-phenanthroline precursor-based material [34,136], as a catalyst in the cyclopropanation of olefins using diazo compounds [178]. Under optimized conditions, the reactions had a broad scope and used 1,2-dimethoxyethane as solvent at 60 °C (Scheme 28). Notably, the authors addressed how to regenerate the catalyst. While heat treatment was somewhat effective, treating the catalyst with a 3% H_2O_2 solution allowed it to replenish its activity fully. This is perhaps due to fouling at the catalyst's surface by concomitant oligomerization of alkenes.

He and co-workers demonstrated using an iron catalyst derived from chitosan in C–N coupling reaction (Scheme 29) [179]. It proceeds via hydrogen abstraction from an amide. The catalyst could be recycled but required thermal reactivation.
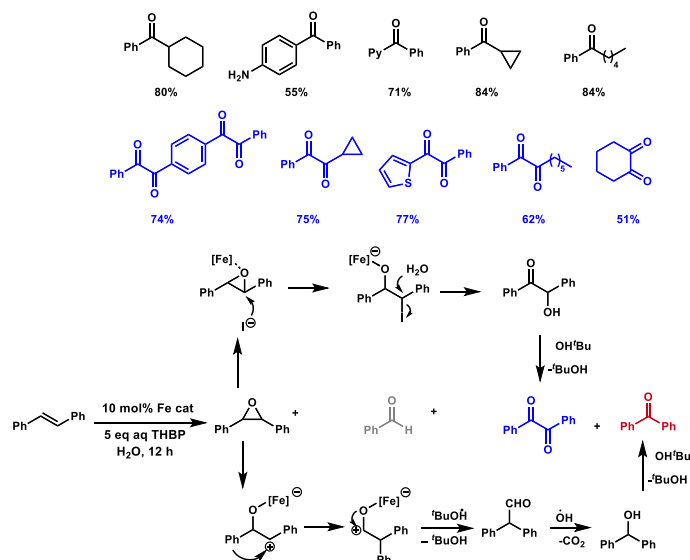
Carbon-carbon bond formation with M–N–C materials as catalysts is rarely reported. Zhang and co-workers reported that Co–N_x sites are responsible for aerobic oxidations of alcohols [180]. When an appropriate combination of primary and secondary alcohols is selected, α,β-unsaturated ketones are obtained as products. Xie et al. demonstrated that the Co–N–C catalyst fabricated by polymerization, pyrolysis, and acid etching of aniline with premixed polyvinylpyrrolidone (PVP) coated SiO_2 nanospheres and Co(OAc)$_2$ [44]. It was able to catalyze reduction alkylation of quinolines and isoquinolines predominantly with arylaldehydes with trifluoracetic acid as an additive (Scheme 30). The authors suggest that cobalt oxides are the catalytic species; however, they are not observed in TEM micrographs. In the case of 2-methylquinoline, a dually alkylated product was observed.

Xie et al. developed a more efficient cobalt catalyst for the dual alkylation of quinolones using aldehydes [181]. It was nitrogen, silicon co-doped and TiO$_2$ supported (Scheme 31). TEM and XRD of the active catalyst CoO$_x$/N-Si-TiO$_2$-800 did not detect metallic cobalt or cobalt oxide NPs.
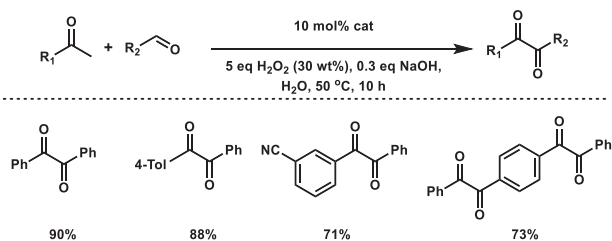
Table 10
Optimization of selective oxidation of alkenes.

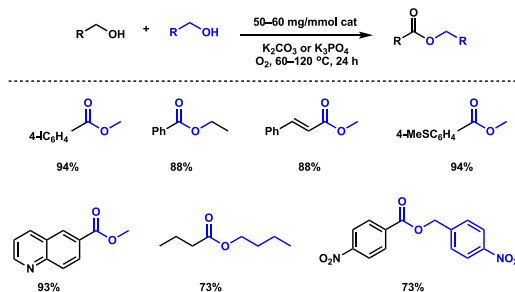| Entry	Catalyst	Conv., %	Selectivity, %		
			Ketone	Aldehyde	Epoxide
1	Fe@NC-800	90	59	17	24
2	Fe@NPC-800	98	92	4	0
3	Fe@NPC-700	79	42	11	47
4	Fe@NPC-900	100	71	11	10
5	Fe powder	11	45	27	28
6	Fe$_2$O$_3$	19	32	0	68
7	Fe$_3$O$_4$	23	30	22	48
8	Fe(NO$_3$)$_3$	7	71	0	29
9	FePO$_4$	11	77	16	7
10[a]	FePc	31	41	22	37

[a] Iron phthalocyanine.

80%   55%   71%   84%   84%

74%   75%   77%   62%   51%

Ph + Ph   10 mol% Fe cat   5 eq aq THBP   H₂O, 12 h

Scheme 21. Oxidation of alkenes to ketones and diketones and proposed mechanism.

10 mol% cat

5 eq H₂O₂ (30 wt%), 0.3 eq NaOH, H₂O, 50 °C, 10 h

90%   88%   71%   73%

Scheme 22. Tandem condensation/Meinwald rearrangement.

50–60 mg/mmol cat

K₂CO₃ or K₃PO₄
O₂, 60–120 °C, 24 h

94%   88%   88%   94%

93%   73%   73%

Scheme 23. Oxidative esterification using Co–N–C catalyst.

Table 11
Optimization of oxidative esterification of benzyl alcohol.

2.5 mol% cat

K₂CO₃, MeOH, O₂
60 °C, 24 h

ligand	complexation	impregnation	carbonization	active catalyst
	Co(OAc)₂ M/L 1:2	Vulcan XC72R	800 °C, Ar	

L1   L3   L4

Entry	Catalyst	Conv.,[a] %	Yield,[a] %
1	–	<2	<1
2	Co(OAc)₂	5	<1
3	Co-L1/C	12	2
4	Co/C-800	20	12
5	**Co-L1/C-800**	**>99**	**97**
6	Co-L3/C-800	80	74
7	Co-L4/C-800	68	60
8	Co-L1/C@Al₂O₃-800	83	79
9	Co-L1/C@TiO₂-800	52	45

[a] Determined by GC analysis.

Another example of carbon–carbon bond formation is benzylic homocoupling, which was recently reported by Ping et al. (Scheme 32) [176]. The authors used a Co–N–C catalyst previously developed for the oxidation of alkylarenes. It could be recycled, provided the solvent-containing product was removed under anhydrous conditions (via syringe) before introducing a batch of starting materials. Aqueous work-up, however, resulted in reduced yields already on the second run.

An interesting example of preferential carbon–carbon bond cleavage is a report on the decarboxylation of fatty acids over a Co–N–C catalyst, which was prepared from melamine and contained Co NPs [182]. Fatty acids and esters were converted primarily to C_{n-1} alkanes via decarboxylation and C_n alkanes as by-products via hydrodeoxygenation (Scheme 33). The ratio of C_{n-1}/C_n increases as the catalyst loading is increased. The spent catalyst (after several rounds of cycling) also gave rise to C_n alcohols. Activated carbon showed the highest activity and selectivity, while supports (TiO₂, ZrO₂, SiO₂, Al₂O₃) did not.

Sahoo et al. used a chitosan-derived cobalt catalyst, which incorporated various nanoparticles (metallic Co, Co₃O₄, and Co NPs covered with oxides) for protodehalogenation of haloarenes and haloalkanes (Scheme 34) [183]. The reaction required triethylamine as an additive and extensive reaction times. The authors demonstrated the application of this reaction in the synthesis of peronatin B, a natural alkaloid, by using bromine as a protecting group.
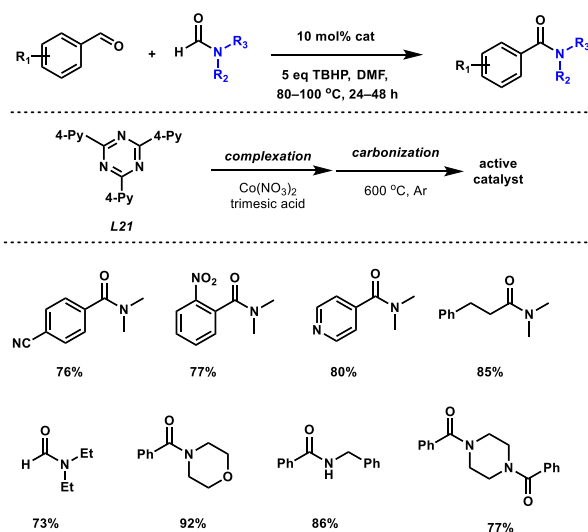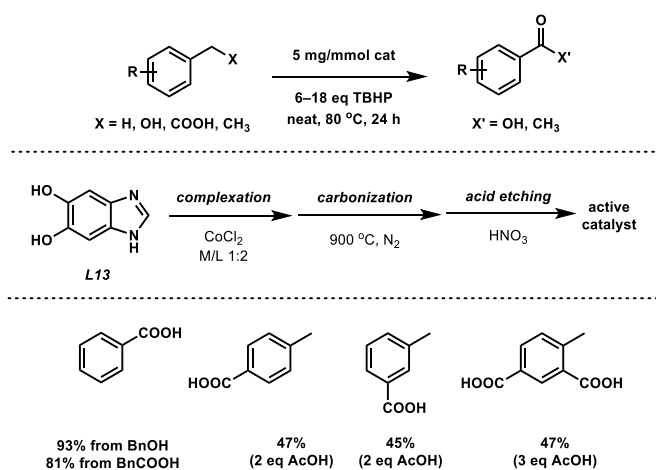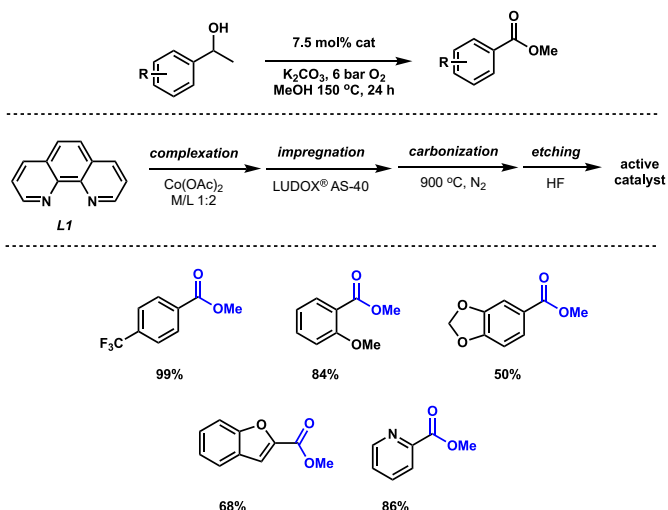
Scheme 24. Substrate scope for the formation of quinazolinones.
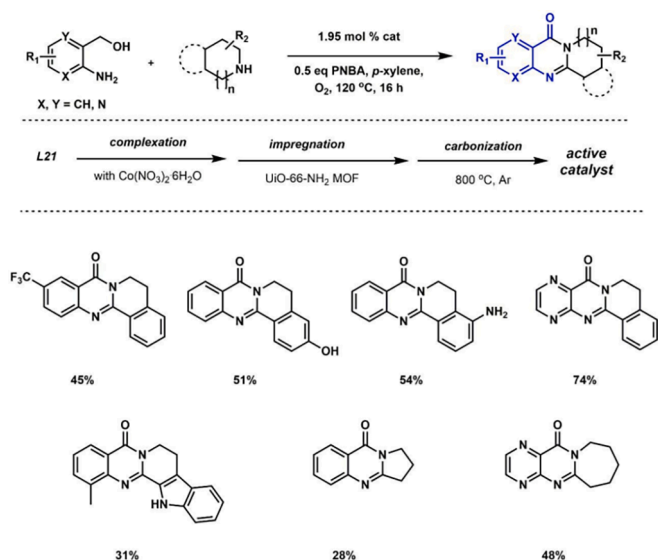
Xie *et al.* demonstrated that Co–N$_x$ sites can catalyze selective sulfonylation of tetrahydroquinoxalines (Scheme 35) [86]. The catalyst was obtained by doping zinc-based MOF ZIF-8 with cobalt, depositing it on a carbon support and carbonizing the material. Iodide, specifically ammonium iodide, was needed to drive the reaction indicating that it is required to generate tetrahydroquinoxalyl radical, which is then trapped by sulfonyl radical to give the desired product.

A variation of "acceptorless" dehydrogenation of amines to give imines (and dihydrogen and ammonia as by-products) was reported to be catalyzed by cobalt material derived by polymerization and carbonization of an imidazolium-based poly-ionic liquid (Scheme 36) [184]. The catalyst contained cobalt(0), cobalt oxides and nitrides, and was highly efficient in this transformation (TON = 165), while alkenes and even alkynes were tolerated.

## 2.6. Nickel based M–N–C materials

Within the iron triad (Fe, Co, Ni), nickel catalysts are less well studied. Often, the nickel systems are used in hydrogenation reactions and typically involve metallic Ni NPs, which are decorated with a thin layer of NiO. In 2016, Pisiewicz *et al.* reported a 1,10-phenanthroline-


Scheme 25. Oxidative esterification from secondary alcohol.

Scheme 26. Oxidation of methylarenes to carboxylic acids.

Scheme 27. Oxidative amidation of aldehydes with N-formamides.

derived nickel catalyst for the reduction of nitroarenes [185]. Akin to **C1** and **C12**, Vulcan XC72R was used as carbon support. Additionally, reductive amination was also promoted (Table 12). It was found that the metallic nickel(0) nanoparticles were decorated with a layer of NiO and embedded into carbon support. The authors suggested that these nanoparticles served as active species. Interestingly, carbonization under NH$_3$ decreased catalyst activity. Nitroarenes were preferentially reduced in the presence of ketones, alkynes and alkenes (Scheme 37), and one equivalent of triethylamine was needed to ensure high yields.

Hahn *et al.* used a combination of nickel salen complex and γ-Al$_2$O$_3$ as support to prepare catalyst **C47**, which was tested for the reductive amination of ketones and aldehydes to primary amines using ammonia (Table 13) [186]. Other supports such as TiO$_2$, SiO$_2$, CeO$_2$ and activated carbon did not show any activity. From XRD patterns and TEM micrographs presence of metallic nickel nanoparticles of a mean size of 8 nm was detected. Moreover, XPS also indicated Ni^{2+} suggesting that Ni–N$_x$ sites were also present. γ-Al$_2$O$_3$ were not fully covered by carbon layers, and these additional sites were important for reactivity. Various groups were tolerated (e.g., iodo, boronyl, alkenes) (Scheme 38).

Yang and co-workers reported a unique nickel-based single-atom catalyst (Table 14) for the reduction of nitroarenes [187]. The authors used MgO as sacrificial support, which was later removed by acid etching. This was done to prevent nickel aggregation into nanoparticles
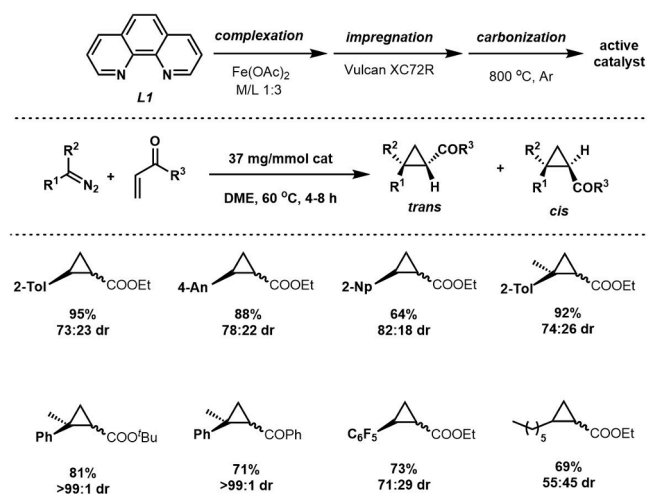
**Scheme 28.** Substrate scope for cyclopropanation of olefins.
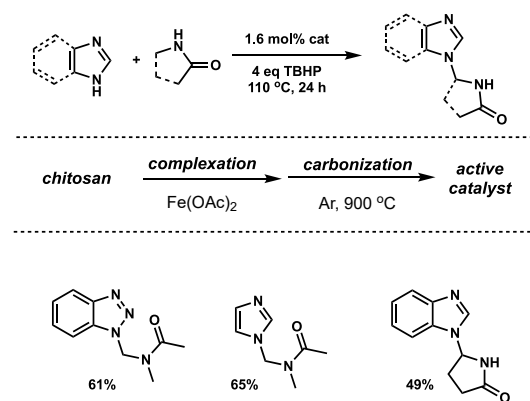
Scheme 29. C–N cross-coupling.

and increase the amount of Ni–N$_x$ sites. The presence of nickel single atoms was determined by HAADF–STEM, XANES and EXAFS. Moreover, higher carbonization temperature at 800 °C led to Ni NPs, protected by carbon shells. Treatment with sodium thiocyanate led to catalyst poisoning. XANES revealed that the valence state of **C48** is between Ni foil and NiPc (nickel phthalocyanine). EXAFS detected only the Ni–N pair (coordination numbers 3.3), indicating that **C48** is atomically dispersed. The DFT calculations also supported that the NiN$_3$ species was the most active. Further evidence of single atom dispersion was given by XPS data showing that the valence state is between 0 and +2. The Ni–N–C catalyst exhibited excellent functional group tolerance with nitriles, alkenes and carboxylic acids remaining. Catalyst stability was
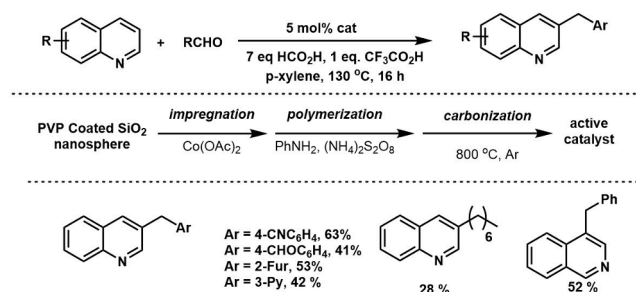
**Scheme 30.** Substrate scope for reductive alkylation.
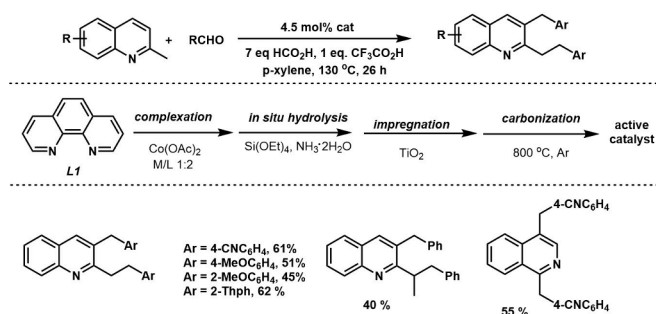
Scheme 31. Substrate scope for reductive alkylation.

not as satisfying since the yield dropped after the third round, and extra time was required to reach higher yields. This may have resulted from metal leaching from the catalyst.

Zhang et al. reported a nickel nanoparticle-based catalyst for selective hydrogenation of nitriles (Scheme 39) [188]. Their mesoporous carbon catalyst was prepared using triblock copolymer Pluronic P123, which was treated with 2,4-dihydroxybenzoic acid, hexamethylenetetramine and ethylenediamine. Nickel was then introduced, followed by pyrolysis under a hydrogen atmosphere. Although the catalyst was shown to be stable for six rounds, its reactivation by treatment under an H$_2$/Ar mixture at 300 °C was necessary. Selectivity towards the formation of primary amines was achieved by adding aqueous ammonia. The active species was shown to be metallic Ni NPs (size 21 nm), which surface was coated by NiO.

Gao et al. reported using atomic layer deposition (ALD) for synthesizing of porous carbon-coated metallic Ni nanoparticles supported on carbon nanofilms generated from polyimide (PI) film carbonization [189]. This material was used for the reductive amination of levulinic acid to 1-benzyl-5-methylpyrrolidine-2-one (Scheme 40). The authors have screened a series of supports (Table 15), which resulted in different acidity of the final catalyst and changes in the distribution of products. No linear relationship was found between the acidity and resulting activity, suggesting that the composition of the catalyst surface and Ni particles played an important role in the process. Excessive coating with polyimide film led to a decrease in activity (entry 4), while catalyst without coating is not stable. Catalysts without PI film coating (Ni@CNTs) and Ni/C (from Ni salt and activated carbon impregnation followed by carbonization) showed poor recyclability due to metal leaching. The most active catalyst could be used for 20 rounds without a drop in yield.
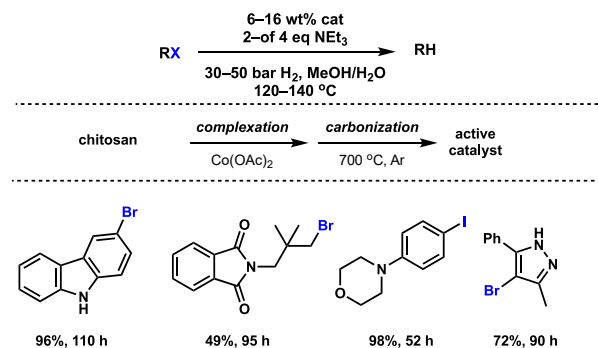
Liu et al. developed a mesoporous catalyst using the polymer Pluronic F127, melamine oligomer as nitrogen source, and formaldehyde
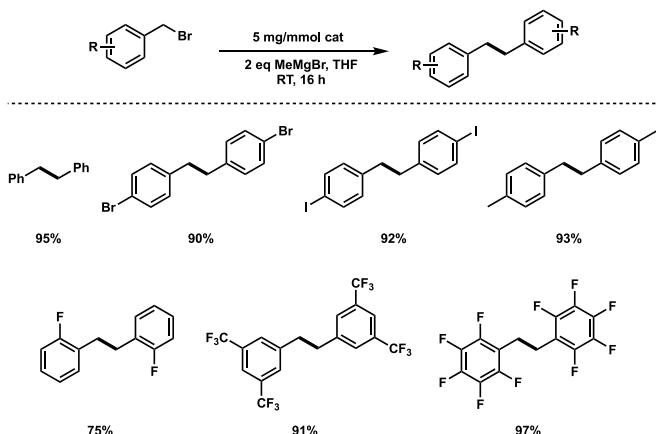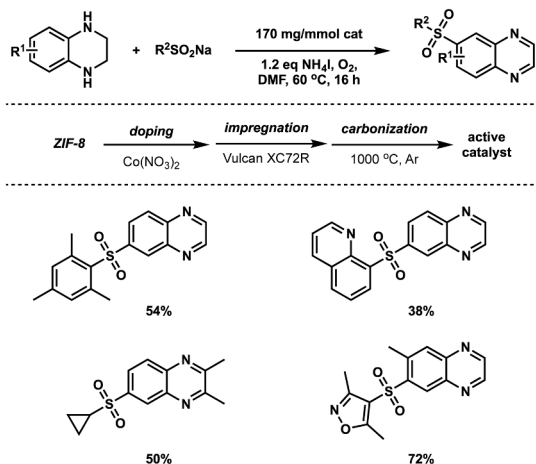
Scheme 32. Substrate scope for oxidation of C–H bond and C–C coupling.
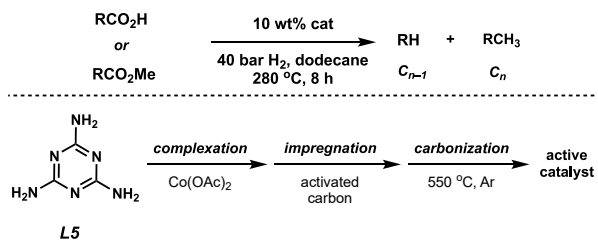
Scheme 33. Decarboxylation of fatty acids and esters.

**Scheme 34.** Protodehalogenation of haloarenes and haloalkanes.

Scheme 35. Selective sulfonylation of tetrahydroquinoxalines.

and phenol, condensed using silica as an emulsifier [190]. After pyrolysis, they obtained hierarchically porous carbon microspheres with metallic nickel NPs embedded into graphitic carbon. The active catalyst contained metallic Ni nanoparticles (22 nm) uniformly dispersed on a carbon support; however, a layer of NiO was detected by XPS. The catalyst prepared without melamine (Ni/CMs) showed comparable activity in the first round (Table 16, entry 5); however, it was unstable.

2.7. Other metal-based M–N–C catalysts

While copper is one of the pinnacles of transition metal catalysis, the carbon-supported examples of copper catalysts reported to date do not explicitly involve nitrogen-doped materials [191–194]. Additionally, these carbon-supported copper materials are also not acid leached, which suggests that various nanoparticles comprising of Cu, Cu$_2$O, and CuO directly adhere to the carbon support and may play a defining role in overall reactivity. The copper examples are summarized below.

Yu et al. profiled a series of heterogeneous catalysts with different
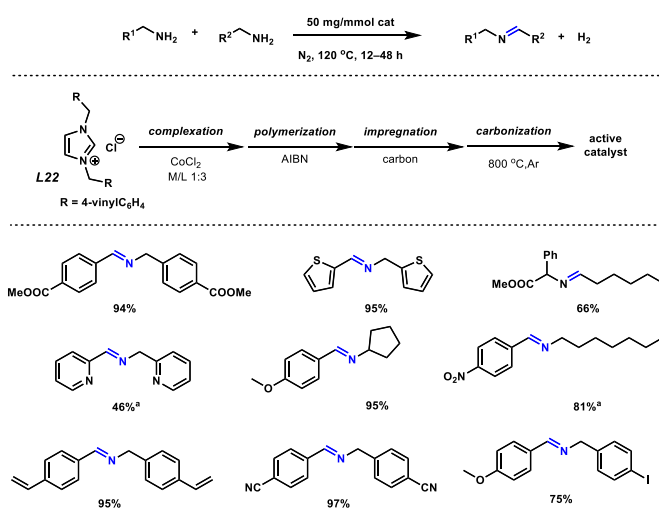
Scheme 36. Acceptorless dehydrogenation of amines.

Table 12
Reductive amination with different nickel-based catalysts.

Entry	Catalyst	Isolated yield, %
1	Co$_3$O$_4$/NGr@C	46
2	Ni-NiO/NGr@C-800	44
3	Ni-NiO/NGr@C-600	40
4[a]	Ni-NiO/NGr@C	30
5[b]	Ni-NiO/NGr@C	42
6[c]	Ni-NiO/NGr@C	10
7	Ni(phen)$_2$@C	trace
8	Vulcan XC72R	trace

[a] 1.5 wt%.
[b] Activated carbon pretreated with H$_2$O$_2$.
[c] Carbonization under NH$_3$.

copper halides supported on coconut shell carbon, which contained a minimal amount of nitrogen (EDS spectra) [191]. Hot filtration test proved that the reaction required the heterogeneous catalyst and that Cu (I) species were employed. The identity of the catalyst sites was not studied.

Sun et al. reported a copper MOF (Cu-TPA) derived two-phase Cu/
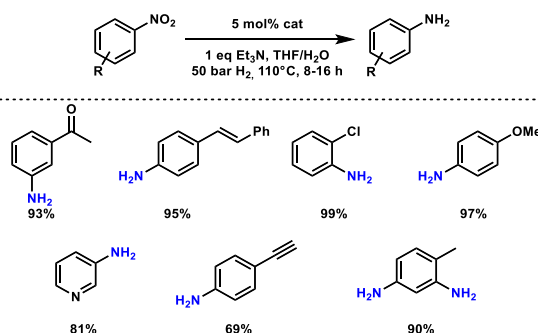
Scheme 37. Substrate scope for hydrogenation of substituted nitroarenes.

Table 13
Optimization for reductive amination.

Entry	Catalyst	Yield, [a] %
1	Ni-**L24**@Al$_2$O$_3$-600	37
2	Ni-**L24**@Al$_2$O$_3$-700	78
3[b]	Ni-**L24**@Al$_2$O$_3$-700	99
4	Ni-**L24**@Al$_2$O$_3$-800	48
5	Ni-**L24**@CeO$_2$-700	36
6	Ni-**L24**@AC-700	0
7	Ni-**L24**@SiO$_2$-700	0
8	Ni-**L24**@TiO$_2$-700	0
9	Ni@Al$_2$O$_3$-700	0

[a] Yields were determined by GC.
[b] 24 mg/mmol loading.

Scheme 38. Substrate scope for reductive amination.

Table 14
Optimization of reduction of nitrobenzene.

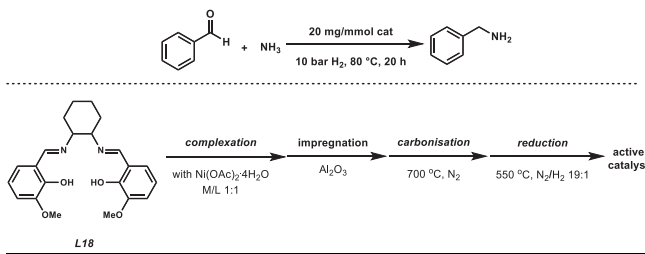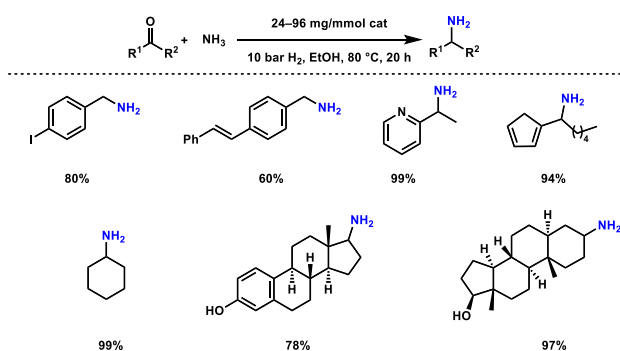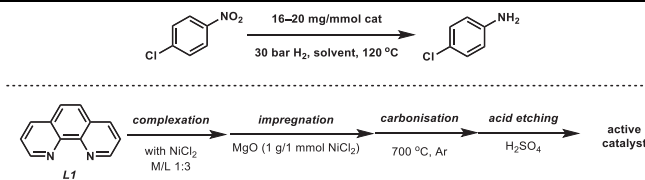| Entry	Catalyst	Loading, mg/mmol	Solvent	Time, h	Yield,[a] %
1	Ni-N-C-700	20	EtOH	8	99
2	Ni-N-C-600	16	EtOH	10	82
3	Ni-N-C-800	16	EtOH	10	63
4	Ni-N-C-700	16	EtOH	10	99
5[b]	Ni-N-C-700	16	EtOH	10	28
6	NiCl$_2$-**L1**	16	EtOH	10	–
7[c]	Ni/NC-700	16	EtOH	10	38
8	Ni-N-C-700	16	H$_2$O	10	85
9	Ni-N-C-700	16	EtOAc	10	43
10	Ni-N-C-700	16	THF	10	13

[a] Isolated yield.
[b] NaSCN added.
[c] Ni/NC-700 was done with NiCl$_2$ supported on oxidized porous carbon with melamine as nitrogen source.

Cu$_2$O@rGO heterogeneous catalyst with reduced graphite oxide as carbon support, showing that the synergy between Cu and Cu$_2$O promotes Sonogashira coupling [192]. Kar and Srivastava profiled a series of similar heterogeneous catalysts based on carbonized HKUST-1 [193]. Again, Cu/Cu$_2$O nanoparticles were formed and utilized for Sonogashira, Ullmann and A^3 coupling reactions. Oxidation of diphenylmethane with N-hydroxyphthalimide as catalyst and O$_2$ as terminal oxidant was reported.

Li et al. recently reported a CuO/Cu$_2$O@Al$_2$O$_3$ heterogeneous catalyst for the hydrogenation of nitroarenes, quinolines, ketones amines and alkynes [194]. Interestingly, they showed that the 1,10-phenanthroline-derived copper catalyst was, however, ineffective.

Several groups reported M–N–C systems based on gold nanoparticles. Liu et al. demonstrated that the electronic properties of N-doped carbon support, derived by "nitriding" activated carbon with urea [195], may define the particle size and reactivity of AuNPs at the surface of a heterogeneous catalyst. AuNPs were grown at the N-doped carbon by performing in situ reduction of HAuCl$_4$ with NaBH4 at various pH. In particular, pH of 3, 7 and 12 lead to catalysts AuNC-6@NC, AuNC-2@NC and AuNC-10@NC, respectively [196].

Ultrasmall NPs have led to higher selectivities in styrene oxidation reaction to epoxide in polar solvents (e.g., MeCN and MeCN/H$_2$O 9:1). In contrats, in apolar solvents such as hexane and toluene, benzaldehyde was the major product. A further set of substrates were examined (Table 17; entries 10–13). However, over time, the NPs at the catalyst's surface began to increase in size, leading to a drop in selectivities.

Fiorio et al. screened a number of supports and nitrogen-containing precursors in selective alkyne hydrogenation (Table 10) [197]. Out of the five precursors and six supports, a combination of 1,10-phenanthroline and TiO$_2$ was the best-performing. The Au/precursor ratio and carbonization at various temperatures were optimized (Table 18, entries 1–4). The active catalyst contained Au NPs with a mean diameter of 4.5 nm. In comparison, the precursor-free catalyst had Au NPs of 17 nm and showed significantly lower activity, suggesting that NP size is important in determining catalytic activity (entry 8).

Au based M–N–C showed excellent selectivity giving cis-alkenes with many groups tolerated (Scheme 41). At higher temperatures, pressure, longer reaction times, and the absence of the alkyne moieties, N-oxides, sulfoxides, epoxides, nitroarenes and aldehydes were reduced.

Li et al. reported a palladium-based heterogeneous catalystthat used chitin-derived nitrogen-doped carbon microspheres as carbon support [198]. Selective hydrogenation of phenylacetylene to styrene was demonstrated with 0.05 mmol% Pd loading at 1 bar H$_2$ in ethanol. This reactivity was achieved by diminishing the absorption of styrene on Pd NPs supported on N-doped carbon through Mott–Schottky effect by decreasing their electron density [172].

Martínez-Prieto and co-workers showed that the presence of basic (nitrogen) sites next to ruthenium NPs (average size of 1.5 nm) leads to highly effective and robust catalysts for the hydrogenation of fatty acids to alcohols [199]. To fabricate the catalyst, they used the Ru(cod)(cot) complex, decomposed in a dihydrogen atmosphere in the presence of N-doped reduced graphene oxide. Non-doped rGO or activated carbon led to lower selectivities. Another example of Ru NPs being smaller on N-doped carbon was reported for acceptorless dehydrogenations [200].

Liu et al. prepared a mesoporous nitrogen-doped platinum catalyst for the decarboxylation of fatty acids to alkanes [201]. They started with melamine, phenol, and formaldehyde to prepare a resin used as a nitrogen source, and tetraethyl orthosilicate and Pluronic F127 were used as a dual template. The final Pt–N–C catalyst material included well-dispersed Pt NPs (2 nm) and was active for at least eight runs, with no reduction in conversions and selectivities.

Guo et al. used bimetallic nanoparticles Ni$_{30}$Pd$_{70}$ supported on N-doped graphene, prepared from melamine and single-layered graphene
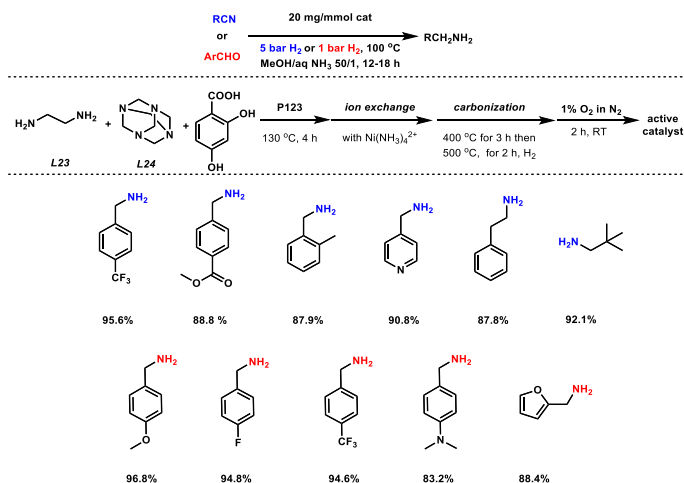
Scheme 39. Substrate scope for selective hydrogenation of nitriles.
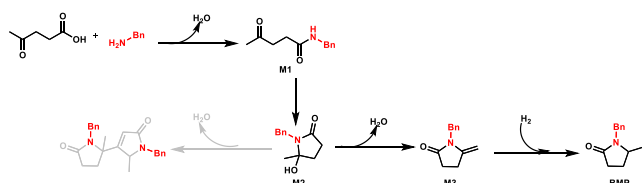
Scheme 40. Proposed mechanism for of reduction of levulinic acid.

Table 15

Optimization of reduction of levulinic acid.

Entry	Catalyst	Yield,[a] %		
		M3	BMP	M4
1	Ni@CNTs	1	99	–
2	CNF$_{10}$@Ni@CNTs	1	99	–
3	CNF$_{30}$@Ni@CNTs	1	99	–
4	CNF$_{50}$@Ni@CNTs	26	72	–
5	Ni/CNTs	8	90	–
6	Ni/C	1	99	–
7	Ni/TiO	33	34	17
8	Ni/NbOPO$_4$	31	42	22
9	Ni/HZSM-5	21	21	36
10	Ni/SAPO-34	24	32	26

[a] Yields were calculated by GC using 1–4 dioxane as internal standard.

Table 16

Optimization of reduction of levulinic acid.
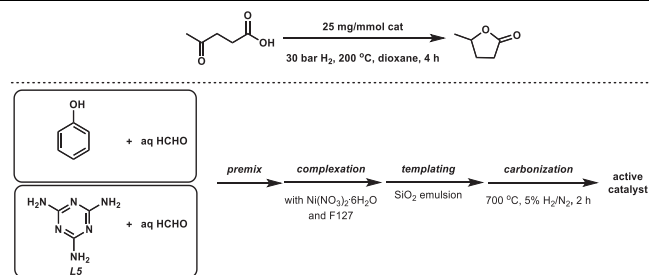
Entry	Catalyst	Conv., %	Selectivity, %
1	NCMs	<1	–
2	Ni@NCMs-600	78	99
3	Ni@NCMs-700	99	99
4	Ni@NCMs-800	36	99
5[a]	Ni@CMs	96	99
6	Ni/AC	80	99

[a] Ni@CMs were prepared using the same conditions as Ni@NCMs except in the absence of melamine.
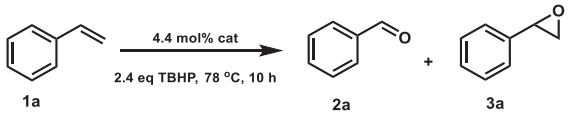
oxide. Using borane ammonia complex, the catalyst was optimized for protodehalogenation of haloarenes, including chlorides [202].

Further examples of noble metal nanoparticles on nitrogen-doped carbon supports were earlier reviewed [29].

3. Conclusions and outlook

M–N–C materials, based on non-precious metals (Fe, Ni, Co, Mn, Cu), are gaining popularity in heterogeneous and electrocatalysis. Their fabrication strategies are similar, albeit acid etching is often omitted in the former case. To date, the choice of applied precursors has remained rather limited and largely relies on the use of 1,10-phenanthroline, porphyrins, phthalocyanines and well-established MOFs (ZIF-8 and

Table 17
Optimization of oxidation of alkenes.

Entry	Catalyst	Solvent	Conv., %	Selectivity, %
1	AuNC-2@NC	MeCN	96.8	40.4
2	AuNC-6@NC	MeCN	55.0	37.8
3	AuNC-10@NC	MeCN	53.7	53.0
4	AuNC-2@NC	MeCN/H$_2$O 9:1	25.3	82.3
5	AuNC-6@NC	MeCN/H$_2$O 9:1	16.6	71.2
6	AuNC-10@NC	MeCN/H$_2$O 9:1	14.8	60.3
7	AuNC-2@NC	hexane	57.2	11.3
8	AuNC-2@NC	EtOH	6.8	100
9	AuNC-2@NC	PhMe	49.8	21.1
10[a]	AuNC-2@NC	MeCN/H$_2$O 9:1	23.5	99.7
11[b]	AuNC-2@NC	MeCN/H$_2$O 9:1	77.1	97.2
12[c]	AuNC-2@NC	MeCN/H$_2$O 9:1	49.2	89.7
13[d]	AuNC-2@NC	MeCN/H$_2$O 9:1	30.6	94.2

[a] 4-methoxystyrene.
[b] 4-methylstyrene.
[c] *a*-methylstyrene.
[d] 1-hexene.

ZIF-67). In the future, it might be more insightful to explore a broader range of precursors and metal combinations to improve the stability and performance of final catalysts. To ensure scientific accuracy and enhance the reliability of M–N–C materials, two common errors must be addressed. First, active site determination should rely on experimental data with positive/negative controls, combined with thorough characterization. Second, conducting long-term stability tests and observing conversion at lower levels are crucial to accurately evaluate catalyst performance. It helps determine the catalyst's performance when it is
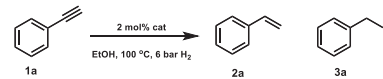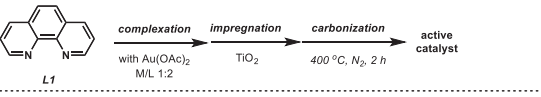
Table 18
Optimization of hydrogenation of alkynes.

Entry	Catalyst	Conv., %	Yield of 2a, %
1	Au–**L1**@TiO$_2$–200	51	>99
2	Au–**L1**@TiO$_2$–400	100	>99
3	Au–**L1**@TiO$_2$–600	27	>99
4	Au–**L1**@TiO$_2$–800	5	65
5	Au–**L2**@TiO$_2$–400	47	88
6	Au–**L25**@TiO$_2$–400	8	79
7	Au–**L27**@TiO$_2$–400	18	94
8	Au–**L28**@TiO$_2$–400	65	93
9	Au–**L29**@TiO$_2$–400	17	89
10[a]	Au–**L1**@TiO$_2$	0	–
11	Au@TiO$_2$	4	>99
12	**L1**@TiO$_2$	0	–
13	Au–**L1**/CeO$_2$–400	6	>99
14	Au–**L1**/MgO–400	4	>99
15	Au–**L1**/Fe$_3$O$_4$–400	3	>99
16	Au–**L1**/SiO$_2$–400	71	65
17	Au–**L1**/C–400	5	>99

[a] Catalyst was not pyrolyzed.
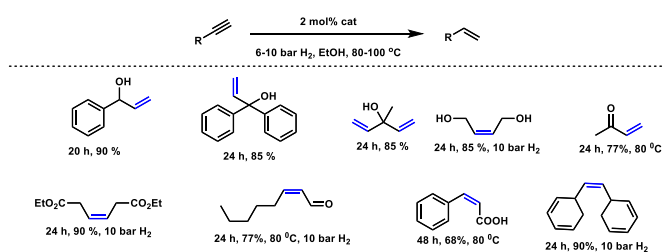
Scheme 41. Substrate scope for semi hydrogenation of alkyne to alkene.

not overloaded or pushed to its limits. This will also be essential for getting more sophisticated computational models and eventually result in the uptake of M–N–C materials for large-scale applications. This, however, will require a deeper understanding of the deactivation mechanisms of the catalysts in hand to reduce their loadings, obtain their environmental toxicity profiles and ensure their sustainability in the long term.

CRediT authorship contribution statement

Kefeng Ping: Conceptualization, Investigation, Visualization, Writing - original draft, Writing - review & editing. **Rohit Bhadoria:** Conceptualization, Investigation, Visualization, Writing - original draft, Writing - review & editing. **Pavel Starkov:** Conceptualization, Investigation, Supervision. **Nadezda Kongi:** Conceptualization, Supervision, Data curation, Funding acquisition, Project administration, Resources, Writing - review & editing.

Declaration of Competing Interest

The authors declare that they have no known competing financial interests or personal relationships that could have appeared to influence the work reported in this paper.

Data availability

Data will be made available on request.

Acknowledgements

References

[1] Z. Shi, W. Yang, Y. Gu, T. Liao, Z. Sun, Metal-nitrogen-doped carbon materials as highly efficient catalysts: progress and rational design, Adv. Sci. 7 (2020), 2001069, https://doi.org/10.1002/advs.202001069.

[2] J. Pei, R. Zhao, X. Mu, J. Wang, C. Liu, X.-D. Zhang, Single-atom nanozymes for biological applications, Biomater. Sci. 8 (2020) 6428–6441, https://doi.org/10.1039/D0BM01447H.

[3] J. Masa, W. Xia, M. Muhler, W. Schuhmann, On the role of metals in nitrogen-doped carbon electrocatalysts for oxygen reduction, Angew. Chem. Int. Ed. 54 (2015) 10102–10120, https://doi.org/10.1002/anie.201500569.

[4] Y.-S. Wei, M. Zhang, R. Zou, Q. Xu, Metal-organic framework-based catalysts with single metal sites, Chem. Rev. 120 (2020) 12089–12174, https://doi.org/10.1021/acs.chemrev.9b00757.

[5] Y. Deng, Y. Xie, K. Zou, X. Ji, Review on recent advances in nitrogen-doped carbons: preparations and applications in supercapacitors, J. Mater. Chem. A. 4 (2016) 1144–1173, https://doi.org/10.1039/C5TA08620E.

[6] T. Asset, P. Atanassov, Iron-nitrogen-carbon catalysts for proton exchange membrane fuel cells, Joule 4 (2020) 33–44, https://doi.org/10.1016/j.joule.2019.12.002.

[7] Y. He, S. Liu, C. Priest, Q. Shi, G. Wu, Atomically dispersed metal–nitrogen–carbon catalysts for fuel cells: advances in catalyst design, electrode performance, and durability improvement, Chem. Soc. Rev. 49 (2020) 3484–3524, https://doi.org/10.1039/C9CS00903E.

[8] Y.P. Zhu, C. Guo, Y. Zheng, S.-Z. Qiao, Surface and interface engineering of noble-metal-free electrocatalysts for efficient energy conversion processes, Acc. Chem. Res. 50 (2017) 915–923, https://doi.org/10.1021/acs.accounts.6b00635.

[9] X. Lu, L. Xiao, P. Yang, H. Xu, L. Liu, R. Li, Y. Li, H. Zhang, J. Zhang, M. An, Highly exposed surface pore-edge FeNx sites for enhanced oxygen reduction performance in Zn-air batteries, Inorg. Chem. Front. 10 (2023) 815–823, https://doi.org/10.1039/D2QI02228A.

[10] Z. Wu, X.F. Lu, S. Zang, X.W. (David) Lou, Non-noble-metal-based electrocatalysts toward the oxygen evolution reaction, Adv. Funct. Mater. 30 (2020), 1910274, https://doi.org/10.1002/adfm.201910274.

[11] A.A. Gewirth, J.A. Varnell, A.M. DiAscro, Nonprecious metal catalysts for oxygen reduction in heterogeneous aqueous systems, Chem. Rev. 118 (2018) 2313–2339, https://doi.org/10.1021/acs.chemrev.7b00335.

[12] W. Wang, Q. Jia, S. Mukerjee, S. Chen, Recent insights into the oxygen-reduction electrocatalysis of Fe/N/C materials, ACS Catal. 9 (2019) 10126–10141, https://doi.org/10.1021/acscatal.9b02583.

[13] U. Martinez, S. Komini Babu, E.F. Holby, H.T. Chung, X. Yin, P. Zelenay, Progress in the development of Fe-based PGM-free electrocatalysts for the oxygen reduction reaction, Adv. Mater. 31 (2019), 1806545, https://doi.org/10.1002/adma.201806545.

[14] S.-N. Zhao, J.-K. Li, R. Wang, J. Cai, S.-Q. Zang, Electronically and geometrically modified single-atom fe sites by adjacent Fe nanoparticles for enhanced oxygen reduction, Adv. Mater. 34 (2022), 2107291, https://doi.org/10.1002/adma.202107291.

[15] M. Tahir, L. Pan, F. Idrees, X. Zhang, L. Wang, J.-J. Zou, Z.L. Wang, Electrocatalytic oxygen evolution reaction for energy conversion and storage: A comprehensive review, Nano Energy 37 (2017) 136–157, https://doi.org/10.1016/j.nanoen.2017.05.022.

[16] F. Dong, M. Cai, Z. Chen, X. Liu, G. Zhang, J. Qiao, S. Sun, Atomically dispersed transition metal-nitrogen-carbon bifunctional oxygen electrocatalysts for zinc-air batteries: recent advances and future perspectives, Nano-Micro Lett. 14 (2021) 36, https://doi.org/10.1007/s40820-021-00768-3.

[17] W. Xu, H. Tang, H. Gu, H. Xi, P. Wu, B. Liang, Q. Liu, W. Chen, Research progress of asymmetrically coordinated single-atom catalysts for electrocatalytic reactions, J. Mater. Chem. A. 10 (2022) 14732–14746, https://doi.org/10.1039/D2TA03034A.

[18] A. Kundu, S. Mallick, S. Ghora, C.R. Raj, Advanced oxygen electrocatalyst for air-breathing electrode in Zn-Air batteries, ACS Appl. Mater. Interfaces 13 (2021) 40172–40199, https://doi.org/10.1021/acsami.1c08462.

[19] L. Zhang, J. Xiao, H. Wang, M. Shao, Carbon-based electrocatalysts for hydrogen and oxygen evolution reactions, ACS Catal. 7 (2017) 7855–7865, https://doi.org/10.1021/acscatal.7b02718.

[20] L.-J. Yuan, X.-L. Sui, C. Liu, Y.-L. Zhuo, Q. Li, H. Pan, Z.-B. Wang, Electrocatalysis mechanism and structure-activity relationship of atomically dispersed metal-nitrogen-carbon catalysts for electrocatalytic reactions, Small Methods. 7 (2023), 2201524, https://doi.org/10.1002/smtd.202201524.

[21] A. Kumar, V.K. Vashistha, D.K. Das, S. Ibraheem, G. Yasin, R. Iqbal, T.A. Nguyen, R.K. Gupta, Md., Rasidul Islam, M-N-C-based single-atom catalysts for H2, O2 & CO2 electrocatalysis: activity descriptors, active sites identification, challenges and prospects, Fuel 304 (2021), 121420, https://doi.org/10.1016/j.fuel.2021.121420.

[22] Y. Wang, X. Cui, L. Peng, L. Li, J. Qiao, H. Huang, J. Shi, Metal–nitrogen–carbon catalysts of specifically coordinated configurations toward typical electrochemical redox reactions, Adv. Mater. 33 (2021) 2100997, https://doi.org/10.1002/adma.202100997.

[23] G. Qing, R. Ghazfar, S.T. Jackowski, F. Habibzadeh, M.M. Ashtiani, C.-P. Chen, M.R. Smith, T.W. Hamann, Recent advances and challenges of electrocatalytic N2 reduction to ammonia, Chem. Rev. 120 (12) (2020) 5437–5516, https://doi.org/10.1021/acs.chemrev.9b00659.

[24] Y. Zhang, Z. Yu, F. She, L. Wei, Z. Zeng, H. Li, Design of molecular MNC dual-atom catalysts for nitrogen reduction starting from surface state analysis, J. Colloid Interface Sci. 640 (2023) 983–989, https://doi.org/10.1016/j.jcis.2023.03.033.

[25] X. Zheng, Y. Liu, Y. Yan, X. Li, Y. Yao, Modulation effect in adjacent dual metal single atom catalysts for electrochemical nitrogen reduction reaction, Chin. Chem. Lett. 33 (2022) 1455–1458, https://doi.org/10.1016/j.cclet.2021.08.102.

[26] T. Tang, Z. Wang, J. Guan, Optimizing the electrocatalytic selectivity of carbon dioxide reduction reaction by regulating the electronic structure of single-atom M-N-C materials, Adv. Funct. Mater. 32 (2022), 2111504, https://doi.org/10.1002/adfm.202111504.

[27] L. Delafontaine, T. Asset, P. Atanassov, Metal–nitrogen–carbon electrocatalysts for CO2 reduction towards syngas generation, ChemSusChem 13 (2020) 1688–1698, https://doi.org/10.1002/cssc.201903281.

[28] Y.-Z. Chen, R. Zhang, L. Jiao, H.-L. Jiang, Metal–organic framework-derived porous materials for catalysis, Coord. Chem. Rev. 362 (2018) 1–23, https://doi.org/10.1016/j.ccr.2018.02.008.

[29] L. He, F. Weniger, H. Neumann, M. Beller, Synthesis, characterization, and application of metal nanoparticles supported on nitrogen-doped carbon: catalysis beyond electrochemistry, Angew. Chem. Int. Ed 55 (2016) 12582–12594, https://doi.org/10.1002/anie.201603198.

[30] Q. Wang, D. Astruc, State of the art and prospects in metal-organic framework (MOF)-based and MOF-derived nanocatalysis, Chem. Rev. 120 (2020) 1438–1511, https://doi.org/10.1021/acs.chemrev.9b00223.

[31] Y. Wang, L. Chen, C.-C. Hou, Y.-S. Wei, Q. Xu, Multiple catalytic sites in MOF-based hybrid catalysts for organic reactions, Org. Biomol. Chem. 18 (2020) 8508–8525, https://doi.org/10.1039/D0OB01729A.

[32] B. Singh, M.B. Gawande, A.D. Kute, R.S. Varma, P. Fornasiero, P. McNeice, R.V. Jagadeesh, M. Beller, R. Zbořil, Single-atom (iron-based) catalysts: synthesis and applications, Chem. Rev. 121 (2021) 13620–13697, https://doi.org/10.1021/acs.chemrev.1c00158.

[33] V.B. Saptal, V. Ruta, M.A. Bajada, G. Vilé, Single-atom catalysis in organic synthesis, Angew. Chem., Int. Ed. 62 (34) (2023), https://doi.org/10.1002/anie.202219306.

[34] R.V. Jagadeesh, A.-E. Surkus, H. Junge, M.-M. Pohl, J. Radnik, J. Rabeah, H. Huan, V. Schünemann, A. Brückner, M. Beller, Nanoscale Fe2O3 -based catalysts for selective hydrogenation of nitroarenes to anilines, Science 342 (2013) 1073–1076, https://doi.org/10.1126/science.1242005.

[35] B. Sahoo, C. Kreyenschulte, G. Agostini, H. Lund, S. Bachmann, M. Scalone, K. Junge, M. Beller, A robust iron catalyst for the selective hydrogenation of substituted (iso)quinolones, Chem. Sci. 9 (2018) 8134–8141, https://doi.org/10.1039/C8SC02744G.

[36] J. Li, J. Liu, H. Zhou, Y. Fu, Catalytic transfer hydrogenation of furfural to furfuryl alcohol over nitrogen-doped carbon-supported iron catalysts, ChemSusChem 9 (2016) 1339–1347, https://doi.org/10.1002/cssc.201600089.

[37] X. Cui, Y. Li, S. Bachmann, M. Scalone, A.-E. Surkus, K. Junge, C. Topf, M. Beller, Synthesis and characterization of iron–nitrogen-doped graphene/core–shell catalysts: efficient oxidative dehydrogenation of N-heterocycles, J. Am. Chem. Soc. 137 (2015) 10652–10658, https://doi.org/10.1021/jacs.5b05674.

[38] R.V. Jagadeesh, H. Junge, M. Beller, "Nanorust"-catalyzed benign oxidation of amines for selective synthesis of nitriles, ChemSusChem 8 (2015) 92–96, https://doi.org/10.1002/cssc.201402613.

[39] W. Liu, L. Zhang, X. Liu, X. Liu, X. Yang, S. Miao, W. Wang, A. Wang, T. Zhang, Discriminating catalytically active FeNx species of atomically dispersed Fe–N–C catalyst for selective oxidation of the C-H bond, J. Am. Chem. Soc. 139 (2017) 10790–10798, https://doi.org/10.1021/jacs.7b05130.

[40] T. Song, Z. Ma, P. Ren, Y. Yuan, J. Xiao, Y. Yang, A bifunctional iron nanocomposite catalyst for efficient oxidation of alkenes to ketones and 1,2-diketones, ACS Catal. 10 (2020) 4617–4629, https://doi.org/10.1021/acscatal.9b05197.

[41] F.A. Westerhaus, R.V. Jagadeesh, G. Wienhöfer, M.-M. Pohl, J. Radnik, A.-E. Surkus, J. Rabeah, K. Junge, H. Junge, M. Nielsen, A. Brückner, M. Beller, Heterogenized cobalt oxide catalysts for nitroarene reduction by pyrolysis of molecularly defined complexes, Nature Chem. 5 (2013) 537–543, https://doi.org/10.1038/nchem.1645.

[42] W. Liu, L. Zhang, W. Yan, X. Liu, X. Yang, S. Miao, W. Wang, A. Wang, T. Zhang, Single-atom dispersed Co–N–C catalyst: structure identification and performance for hydrogenative coupling of nitroarenes, Chem. Sci. 7 (2016) 5758–5764, https://doi.org/10.1039/C6SC02105K.

[43] P. Zhou, Z. Zhang, One-pot reductive amination of carbonyl compounds with nitro compounds by transfer hydrogenation over Co–Nx as catalyst, ChemSusChem 10 (2017) 1892–1897, https://doi.org/10.1002/cssc.201700348.

[44] F. Xie, R. Xie, J.-X. Zhang, H.-F. Jiang, L. Du, M. Zhang, Direct reductive quinolyl β-C–H alkylation by multispherical cavity carbon-supported cobalt oxide nanocatalysts, ACS Catal. 7 (2017) 4780–4785, https://doi.org/10.1021/acscatal.7b01337.

[45] F. Chen, A.-E. Surkus, L. He, M.-M. Pohl, J. Radnik, C. Topf, K. Junge, M. Beller, Selective catalytic hydrogenation of heteroarenes with N -graphene-modified cobalt nanoparticles (Co3O4–Co/NGr@α-Al2O3), J. Am. Chem. Soc. 137 (2015) 11718–11724, https://doi.org/10.1021/jacs.5b06496.

[46] F. Chen, W. Li, B. Sahoo, C. Kreyenschulte, G. Agostini, H. Lund, K. Junge, M. Beller, Hydrogenation of pyridines using a nitrogen-modified titania-supported cobalt catalyst, Angew. Chem. Int. Ed. 57 (2018) 14488–14492, https://doi.org/10.1002/anie.201803426.

[47] F. Chen, C. Kreyenschulte, J. Radnik, H. Lund, A.-E. Surkus, K. Junge, M. Beller, Selective semihydrogenation of alkynes with N-graphitic-modified cobalt nanoparticles supported on silica, ACS Catal. 7 (2017) 1526–1532, https://doi.org/10.1021/acscatal.6b03140.

[48] H. Luo, L. Wang, S. Shang, G. Li, Y. Lv, S. Gao, W. Dai, Cobalt nanoparticles-catalyzed widely applicable successive C–C bond cleavage in alcohols to access esters, Angew. Chem. Int. Ed. 59 (2020) 19268–19274, https://doi.org/10.1002/anie.202008261.

[49] W. Zhong, H. Liu, C. Bai, S. Liao, Y. Li, Base-free oxidation of alcohols to esters at room temperature and atmospheric conditions using nanoscale Co-based catalysts, ACS Catal. 5 (2015) 1850–1856, https://doi.org/10.1021/cs502101c.

[50] H. Chen, K. Shen, Q. Mao, J. Chen, Y. Li, Nanoreactor of MOF-derived yolk-shell Co@C–N: precisely controllable structure and enhanced catalytic activity, ACS Catal. 8 (2018) 1417–1426, https://doi.org/10.1021/acscatal.7b03270.

[51] R. Nie, J. Chen, M. Chen, Z. Qi, T.-W. Goh, T. Ma, L. Zhou, Y. Pei, W. Huang, Aerobic oxidation of the C-H bond under ambient conditions using highly dispersed Co over highly porous N-doped carbon, Green Chem. 21 (2019) 1461–1466, https://doi.org/10.1039/C8GC03653E.

[52] C. Bai, X. Yao, Y. Li, Easy access to amides through aldehydic C-H bond functionalization catalyzed by heterogeneous Co-based catalysts, ACS Catal. 5 (2015) 884–891, https://doi.org/10.1021/cs501822r.

[53] J.S. Bates, M.R. Johnson, F. Khamespanah, T.W. Root, S.S. Stahl, Heterogeneous M-N-C catalysts for aerobic oxidation reactions: lessons from oxygen reduction electrocatalysts, Chem. Rev. 123 (9) (2023) 6233–6256, https://doi.org/10.1021/acs.chemrev.2c00424.

[54] T.P. Yoon, E.N. Jacobsen, Privileged chiral catalysts, Science 299 (2003) 1691–1693, https://doi.org/10.1126/science.1083622.

[55] A. Wang, J. Li, T. Zhang, Heterogeneous single-atom catalysis, Nat Rev Chem. 2 (2018) 65–81, https://doi.org/10.1038/s41570-018-0010-1.

[56] Y. Wang, H. Su, Y. He, L. Li, S. Zhu, H. Shen, P. Xie, X. Fu, G. Zhou, C. Feng, D. Zhao, F. Xiao, X. Zhu, Y. Zeng, M. Shao, S. Chen, G. Wu, J. Zeng, C. Wang, Advanced electrocatalysts with single-metal-atom active sites, Chem. Rev. 120 (2020) 12217–12314, https://doi.org/10.1021/acs.chemrev.0c00594.

[57] L. Bai, C.-S. Hsu, D.T.L. Alexander, H.M. Chen, X. Hu, A cobalt-iron double-atom catalyst for the oxygen evolution reaction, J. Am. Chem. Soc. 141 (2019) 14190–14199, https://doi.org/10.1021/jacs.9b05268.

[58] J. Wang, Z. Huang, W. Liu, C. Chang, H. Tang, Z. Li, W. Chen, C. Jia, T. Yao, S. Wei, Y. Wu, Y. Li, Design of N-coordinated dual-metal sites: A stable and active Pt-free catalyst for acidic oxygen reduction reaction, J. Am. Chem. Soc. 139 (2017) 17281–17284, https://doi.org/10.1021/jacs.7b10385.

[59] K. Wang, J. Liu, Z. Tang, L. Li, Z. Wang, M. Zubair, F. Ciucci, L. Thomsen, J. Wright, N.M. Bedford, Establishing structure/property relationships in atomically dispersed Co–Fe dual site M-N$_x$ catalysts on microporous carbon for the oxygen reduction reaction, J. Mater. Chem. A. 9 (2021) 13044–13055, https://doi.org/10.1039/D1TA02925H.

[60] M. Ahn, I.Y. Cha, J. Cho, H.C. Ham, Y.-E. Sung, S.J. Yoo, Rhodium-tin binary nanoparticle—A strategy to develop an alternative electrocatalyst for oxygen reduction, ACS Catal. 7 (2017) 5796–5801, https://doi.org/10.1021/acscatal.7b02402.

[61] T. Jayaraman, A.P. Murthy, V. Elakkiya, S. Chandrasekaran, P. Nithyadharseni, Z. Khan, R.A. Senthil, R. Shanker, M. Raghavender, P. Kuppusami, M. Jagannathan, M. Ashokkumar, Recent development on carbon based heterostructures for their applications in energy and environment: A review, J. Ind. Eng. Chem. 64 (2018) 16–59, https://doi.org/10.1016/j.jiec.2018.02.029.

[62] H. Su, K.-X. Zhang, B. Zhang, H.-H. Wang, Q.-Y. Yu, X.-H. Li, M. Antonietti, J.-S. Chen, Activating cobalt nanoparticles via the Mott-Schottky effect in nitrogen-rich carbon shells for base-free aerobic oxidation of alcohols to esters, J. Am. Chem. Soc. 139 (2017) 811–818, https://doi.org/10.1021/jacs.6b10710.

[63] X. Zhan, C. Si, J. Zhou, Z. Sun, MXene and MXene-based composites: synthesis, properties and environment-related applications, Nanoscale Horiz. 5 (2020) 235–258, https://doi.org/10.1039/C9NH00571D.

[64] W. Wang, W. Chen, P. Miao, J. Luo, Z. Wei, S. Chen, NaCl crystallites as dual-functional and water-removable templates to synthesize a three-dimensional graphene-like macroporous Fe-N-C catalyst, ACS Catal. 7 (2017) 6144–6149, https://doi.org/10.1021/acscatal.7b01695.

[65] N. Kazimova, K. Ping, M. Alam, M. Danilson, M. Merisalu, J. Aruväli, P. Paiste, M. Käärik, V. Mikli, J. Leis, K. Tammeveski, P. Starkov, N. Kongi, Shungite-derived graphene as a carbon support for bifunctional oxygen electrocatalysts, J. Catal. 395 (2021) 178–187, https://doi.org/10.1016/j.jcat.2021.01.004.

[66] L. Wang, Z. Sofer, M. Pumera, Will any crap we put into graphene increase its electrocatalytic effect? ACS Nano 14 (2020) 21–25, https://doi.org/10.1021/acsnano.9b00184.

[67] J. Huang, B. Zhao, T. Liu, J. Mou, Z. Jiang, J. Liu, H. Li, M. Liu, Wood-derived materials for advanced electrochemical energy storage devices, Adv. Funct. Mater. 29 (2019), 1902255, https://doi.org/10.1002/adfm.201902255.

[68] I.L. Alonso-Lemus, M.Z. Figueroa-Torres, D. Lardizabal-Gutiérrez, P. Bartolo-Pérez, J.C. Carrillo-Rodríguez, F.J. Rodríguez-Varela, Converting chicken manure into highly active N-P co-doped metal-free biocarbon electrocatalysts: effect of chemical treatment on their catalytic activity for the ORR, Sustainable, Energy Fuels. 3 (2019) 1307–1316, https://doi.org/10.1039/C8SE00583D.

[69] W. Yang, J. Li, D. Ye, X. Zhu, Q. Liao, Bamboo charcoal as a cost-effective catalyst for an air-cathode of microbial fuel cells, Electrochim. Acta 224 (2017) 585–592, https://doi.org/10.1016/j.electacta.2016.12.046.

[70] W. Meng, X. Bai, B. Wang, Z. Liu, S. Lu, B. Yang, Biomass-derived carbon dots and their applications, Energy Environ. Mater. 2 (2019) 172–192, https://doi.org/10.1002/eem2.12038.

[71] P. Veerakumar, I. Panneer Muthuselvam, C.-T. Hung, K.-C. Lin, F.-C. Chou, S.-B. Liu, Biomass-derived activated carbon supported Fe$_3$O$_4$ nanoparticles as recyclable catalysts for reduction of nitroarenes, ACS Sustain. Chem. Eng. 4 (2016) 6772–6782, https://doi.org/10.1021/acssuschemeng.6b01727.

[72] J.Y. Cheon, T. Kim, Y. Choi, H.Y. Jeong, M.G. Kim, Y.J. Sa, J. Kim, Z. Lee, T.-H. Yang, K. Kwon, O. Terasaki, G.-G. Park, R.R. Adzic, S.H. Joo, Ordered mesoporous porphyrinic carbons with very high electrocatalytic activity for the oxygen reduction reaction, Sci Rep. 3 (2013), 2715, https://doi.org/10.1038/srep02715.

[73] A. Bonakdarpour, R.T. Tucker, M.D. Fleischauer, N.A. Beckers, M.J. Brett, D.P. Wilkinson, Nanopillar niobium oxides as support structures for oxygen reduction electrocatalysts, Electrochim. Acta 85 (2012) 492–500, https://doi.org/10.1016/j.electacta.2012.08.005.

[74] J. Zhang, X. Liu, A. Xing, J. Liu, Template-oriented synthesis of nitrogen-enriched porous carbon nanowhisker by hollow TiO$_2$ spheres nanothorns for methanol electrooxidation, ACS Appl. Energy Mater. 1 (2018) 2758–2768, https://doi.org/10.1021/acsaem.8b00420.

[75] Z. Zhang, J. Liu, J. Gu, L. Su, L. Cheng, An overview of metal oxide materials as electrocatalysts and supports for polymer electrolyte fuel cells, Energy Environ. Sci. 7 (2014) 2535–2558, https://doi.org/10.1039/C3EE43886D.

[76] C. Shen, S. Jie, H. Chen, Z. Liu, The Co-N-C catalyst synthesized with a hard-template and etching method to achieve well-dispersed active sites for ethylbenzene oxidation, Front. Chem. 7 (2019), 426, https://doi.org/10.3389/fchem.2019.00426.

[77] Y. Kamitaka, T. Takeshita, Y. Morimoto, MgO-templated mesoporous carbon as a catalyst support for polymer electrolyte fuel cells, Catalysts 8 (2018), 230, https://doi.org/10.3390/catal8060230.

[78] X. Lu, H. Xu, P. Yang, L. Xiao, Y. Li, J. Ma, R. Li, L. Liu, A. Liu, V. Kondratiev, O. Levin, J. Zhang, M. An, Zinc-assisted MgO template synthesis of porous carbon-supported Fe-Nx sites for efficient oxygen reduction reaction catalysis in Zn-air batteries, Appl. Catal. B 313 (2022), 121454, https://doi.org/10.1016/j.apcatb.2022.121454.

[79] B.-C. Hu, Z.-Y. Wu, S.-Q. Chu, H.-W. Zhu, H.-W. Liang, J. Zhang, S.-H. Yu, SiO$_2$-protected shell mediated templating synthesis of Fe–N-doped carbon nanofibers and their enhanced oxygen reduction reaction performance, Energy Environ. Sci. 11 (2018) 2208–2215, https://doi.org/10.1039/C8EE00673C.

[80] A. Serov, M.H. Robson, K. Artyushkova, P. Atanassov, Templated non-PGM cathode catalysts derived from iron and poly(ethyleneimine) precursors, Appl. Catal. B 127 (2012) 300–306, https://doi.org/10.1016/j.apcatb.2012.08.040.

[81] H. Xu, D. Wang, P. Yang, L. Du, X. Lu, R. Li, L. Liu, J. Zhang, M. An, A hierarchically porous Fe-N-C synthesized by dual melt-salt-mediated template as advanced electrocatalyst for efficient oxygen reduction in zinc-air battery, Appl. Catal. B 305 (2022), 121040, https://doi.org/10.1016/j.apcatb.2021.121040.

[82] S. Naumann, Strategies for pore-diameter control in mesoporous carbons derived from organic self-assembly processes, Org. Mater. 03 (2021) 283–294, https://doi.org/10.1055/a-1458-5109.

[83] E. Pérez-Mayoral, I. Matos, M. Bernardo, I. Fonseca, New and advanced porous carbon materials in fine chemical synthesis. Emerging precursors of porous carbons, Catalysts 9 (2019) 133, https://doi.org/10.3390/catal9020133.

[84] Y.V. Kaneti, J. Tang, R.R. Salunkhe, X. Jiang, A. Yu, K.-C.-W. Wu, Y. Yamauchi, Nanoarchitectured design of porous materials and nanocomposites from metal-organic frameworks, Adv. Mater. 29 (2017), 1604898, https://doi.org/10.1002/adma.201604898.

[85] W. Xia, A. Mahmood, R. Zou, Q. Xu, Metal–organic frameworks and their derived nanostructures for electrochemical energy storage and conversion, Energy Environ. Sci. 8 (2015) 1837–1866, https://doi.org/10.1039/C5EE00762C.

[86] F. Xie, G.-P. Lu, R. Xie, Q.-H. Chen, H.-F. Jiang, M. Zhang, MOF-derived subnanometer cobalt catalyst for selective C-H oxidative sulfonylation of tetrahydroquinoxalines with sodium sulfinates, ACS Catal. 9 (2019) 2718–2724, https://doi.org/10.1021/acscatal.9b00037.

[87] A.L. Bouwkamp-Wijnoltz, W. Visscher, J.A.R. van Veen, E. Boellaard, A.M. van der Kraan, S.C. Tang, On active-site heterogeneity in pyrolyzed carbon-supported iron porphyrin catalysts for the electrochemical reduction of oxygen: an in situ Mössbauer study, J. Phys. Chem. B. 106 (2002) 12993–13001, https://doi.org/10.1021/jp0266087.

[88] J.A.R. Van Veen, J.F. Van Baar, K.J. Kroese, Effect of heat treatment on the performance of carbon-supported transition-metal chelates in the electrochemical reduction of oxygen, J. Chem. Soc., Faraday Trans. 1 (77) (1981), 2827, https://doi.org/10.1039/f19817702827.

[89] D.A. Scherson, S.L. Gupta, C. Fierro, E.B. Yeager, M.E. Kordesch, J. Eldridge, R.W. Hoffman, J. Blue, Cobalt tetramethoxyphenyl porphyrin—emission Mössbauer spectroscopy and O2 reduction electrochemical studies, Electrochim. Acta 28 (1983) 1205–1209, https://doi.org/10.1016/0013-4686(83)85006-3.

[90] R. Chen, H. Li, D. Chu, G. Wang, Unraveling oxygen reduction reaction mechanisms on carbon-supported Fe-phthalocyanine and Co-phthalocyanine catalysts in alkaline solutions, J. Phys. Chem. C. 113 (2009) 20689–20697, https://doi.org/10.1021/jp906408y.

[91] V.S. Bagotzky, M.R. Tarasevich, K.A. Radyushkina, O.A. Levina, S.I. Andrusyova, Electrocatalysis of the oxygen reduction process on metal chelates in acid electrolyte, J. Power Sources 2 (1978) 233–240, https://doi.org/10.1016/0378-7753(78)85014-9.

[92] M. Lefèvre, E. Proietti, F. Jaouen, J.-P. Dodelet, Iron-based catalysts with improved oxygen reduction activity in polymer electrolyte fuel cells, Science 324 (2009) 71–74, https://doi.org/10.1126/science.1170051.

[93] B.Y. Xia, Y. Yan, N. Li, H.B. Wu, X.W. (David) Lou, X. Wang, A metal–organic framework-derived bifunctional oxygen electrocatalyst, Nat. Energy 1 (2016) 1–8, https://doi.org/10.1038/nenergy.2015.6.

[94] H. Yin, C. Zhang, F. Liu, Y. Hou, Hybrid of iron nitride and nitrogen-doped graphene aerogel as synergistic catalyst for oxygen reduction reaction, Adv. Funct. Mater. 24 (20) (2014) 2930–2937, https://doi.org/10.1002/adfm.201303902.

[95] P. Zhou, L. Jiang, F. Wang, K. Deng, K. Lv, Z. Zhang, High performance of a cobalt–nitrogen complex for the reduction and reductive coupling of nitro compounds into amines and their derivatives, Sci. Adv. 3 (2017), e1601945, https://doi.org/10.1126/sciadv.1601945.

[96] Y. Yuan, Q. Zhang, L. Yang, L. Wang, W. Shi, P. Liu, R. Gao, L. Zheng, Z. Chen, Z. Bai, Facet strain strategy of atomically dispersed Fe·N·C catalyst for efficient oxygen electrocatalysis, Adv. Funct. Mater. 32 (2022), 2206081, https://doi.org/10.1002/adfm.202206081.

[97] H. Liu, L. Chen, C.-C. Hou, Y.-S. Wei, Q. Xu, Soluble porous carbon cage-encapsulated highly active metal nanoparticle catalysts, J. Mater. Chem. A. 9 (2021) 13670–13677, https://doi.org/10.1039/D1TA01352A.

[98] Y. Chen, S. Ji, Y. Wang, J. Dong, W. Chen, Z. Li, R. Shen, L. Zheng, Z. Zhuang, D. Wang, Y. Li, Isolated single iron atoms anchored on N-doped porous carbon as

an efficient electrocatalyst for the oxygen reduction reaction, Angew. Chem. Int. Ed. 56 (2017) 6937–6941, https://doi.org/10.1002/anie.201702473.

[99] Q. Zhou, J. Cai, Z. Zhang, R. Gao, B. Chen, G. Wen, L. Zhao, Y. Deng, H. Dou, X. Gong, Y. Zhang, Y. Hu, A. Yu, X. Sui, Z. Wang, Z. Chen, A Gas-phase migration strategy to synthesize atomically dispersed Mn-N-C catalysts for Zn–air batteries, Small Methods 5 (2021) 2100024, https://doi.org/10.1002/smtd.202100024.

[100] S. Wang, P. Zhou, L. Zhou, F. Lv, Y. Sun, Q. Zhang, L. Gu, H. Yang, S. Guo, A unique gas-migration, trapping, and emitting strategy for high-loading single atomic Cd sites for carbon dioxide electroreduction, Nano Lett. 21 (2021) 4262–4269, https://doi.org/10.1021/acs.nanolett.1c00432.

[101] J. Li, L. Jiao, E. Wegener, L.L. Richard, E. Liu, A. Zitolo, M.T. Sougrati, S. Mukerjee, Z. Zhao, Y. Huang, F. Yang, S. Zhong, H. Xu, A.J. Kropf, F. Jaouen, D. J. Myers, Q. Jia, Evolution pathway from iron compounds to Fe1(II)–N4 sites through gas-phase iron during pyrolysis, J. Am. Chem. Soc. 142 (2020) 1417–1423, https://doi.org/10.1021/jacs.9b11197.

[102] L. Jiao, J. Li, L.L. Richard, Q. Sun, T. Stracensky, E. Liu, M.T. Sougrati, Z. Zhao, F. Yang, S. Zhong, H. Xu, S. Mukerjee, Y. Huang, D.A. Cullen, J.H. Park, M. Ferrandon, D.J. Myers, F. Jaouen, Q. Jia, Chemical vapour deposition of Fe–N–C oxygen reduction catalysts with full utilization of dense Fe–N4 sites, Nat. Mater. 20 (2021) 1385–1391, https://doi.org/10.1038/s41563-021-01030-2.

[103] A. Mehmood, J. Pampel, G. Ali, H.Y. Ha, F. Ruiz-Zepeda, T.-P. Fellinger, Facile metal coordination of active site imprinted nitrogen doped carbons for the conservative preparation of non-noble metal oxygen reduction electrocatalysts, Adv. Energy Mater. 8 (2018), 1701771, https://doi.org/10.1002/aenm.201701771.

[104] D. Menga, F. Ruiz-Zepeda, L. Moriau, M. Šala, F. Wagner, B. Koyutürk, M. Bele, U. Petek, N. Hodnik, M. Gaberšček, T.-P. Fellinger, Active-site imprinting: preparation of Fe–N–C catalysts from zinc ion-templated ionothermal nitrogen-doped carbons, Adv. Energy Mater. 9 (2019), 1902412, https://doi.org/10.1002/aenm.201902412.

[105] D. Menga, J.L. Low, Y.-S. Li, I. Arčon, B. Koyutürk, F. Wagner, F. Ruiz-Zepeda, M. Gaberšček, B. Paulus, T.-P. Fellinger, Resolving the dilemma of Fe–N–C catalysts by the selective synthesis of tetrapyrrolic active sites via an imprinting strategy, J. Am. Chem. Soc. 143 (2021) 18010–18019, https://doi.org/10.1021/jacs.1c04884.

[106] A. Mehmood, M. Gong, F. Jaouen, A. Roy, A. Zitolo, A. Khan, M.-T. Sougrati, M. Primbs, A.M. Bonastre, D. Fongalland, G. Drazic, P. Strasser, A. Kucernak, High loading of single atomic iron sites in Fe–NC oxygen reduction catalysts for proton exchange membrane fuel cells, Nat. Catal. 5 (2022) 311–323, https://doi.org/10.1038/s41929-022-00772-9.

[107] M. Gong, A. Mehmood, B. Ali, K.-W. Nam, A. Kucernak, Oxygen reduction reaction activity in non-precious single-atom (M–N/C) catalysts–contribution of metal and carbon/nitrogen framework-based sites, ACS Catal. 13 (2023) 6661–6674, https://doi.org/10.1021/acscatal.3c00356.

[108] J.S. Bates, F. Khamespanah, D.A. Cullen, A.A. Al-Omari, M.N. Hopkins, J. J. Martinez, T.W. Root, S.S. Stahl, Molecular catalyst synthesis strategies to prepare atomically dispersed Fe-N-C heterogeneous catalysts, J Am Chem Soc. 144 (2022) 18797–18802, https://doi.org/10.1021/jacs.2c08884.

[109] H. Fei, R. Ye, G. Ye, Y. Gong, Z. Peng, X. Fan, E.L.G. Samuel, P.M. Ajayan, J. M. Tour, Boron- and nitrogen-doped graphene quantum dots/graphene hybrid nanoplatelets as efficient electrocatalysts for oxygen reduction, ACS Nano 8 (2014) 10837–10843, https://doi.org/10.1021/nn504637y.

[110] J. Zhao, Z. Chen, Carbon-doped boron nitride nanosheet: an efficient metal-free electrocatalyst for the oxygen reduction reaction, J. Phys. Chem. C. 119 (2015) 26348–26354, https://doi.org/10.1021/acs.jpcc.5b09037.

[111] X. Long, Z. Li, G. Gao, P. Sun, J. Wang, B. Zhang, J. Zhong, Z. Jiang, F. Li, Graphitic phosphorus coordinated single Fe atoms for hydrogenative transformations, Nat. Commun. 11 (2020), 4074, https://doi.org/10.1038/s41467-020-17903-0.

[112] K. Yuan, D. Lützenkirchen-Hecht, L. Li, L. Shuai, Y. Li, R. Cao, M. Qiu, X. Zhuang, M.K.H. Leung, Y. Chen, U. Scherf, Boosting oxygen reduction of single iron active sites via geometric and electronic engineering: nitrogen and phosphorus dual coordination, J. Am. Chem. Soc. 142 (2020) 2404–2412, https://doi.org/10.1021/jacs.9b11852.

[113] S.H. Ahn, A. Manthiram, Cobalt phosphide coupled with heteroatom-doped nanocarbon hybrid electrocatalysts for efficient, long-life rechargeable zinc-air batteries, Small 13 (2017), 1702068, https://doi.org/10.1002/smll.201702068.

[114] G. Lin, Q. Wang, X. Yang, Z. Cai, Y. Xiong, B. Huang, Preparation of phosphorus-doped porous carbon for high performance supercapacitors by one-step carbonization, RSC Adv. 10 (2020) 17768–17776, https://doi.org/10.1039/D0RA02398A.

[115] W. Xi, G. Yan, Z. Lang, Y. Ma, H. Tan, H. Zhu, Y. Wang, Y. Li, Oxygen-doped nickel iron phosphide nanocube arrays grown on ni foam for oxygen evolution electrocatalysis, Small 14 (2018), 1802204, https://doi.org/10.1002/smll.201802204.

[116] X. Lin, S. Jie, Z. Liu, Sulfur and nitrogen-doped porous cobalt carbon catalyst for high efficient aerobic oxidation of hydrocarbons, Mol. Catal. 455 (2018) 143–149, https://doi.org/10.1016/j.mcat.2018.05.031.

[117] L. Fu, Y. Chen, S. Zhao, Z. Liu, R. Zhu, Sulfur-mediated synthesis of N-doped carbon supported cobalt catalysts derived from cobalt porphyrin for ethylbenzene oxidation, RSC Adv. 6 (2016) 19482–19491, https://doi.org/10.1039/C5RA26509F.

[118] S. Yang, L. Peng, E. Oveisi, S. Bulut, D.T. Sun, M. Asgari, O. Trukhina, W. L. Queen, MOF-derived cobalt phosphide/carbon nanocubes for selective hydrogenation of nitroarenes to anilines, Chem. Eur. J. 24 (2018) 4234–4238, https://doi.org/10.1002/chem.201705400.

[119] K. Hu, L. Tao, D. Liu, J. Huo, S. Wang, Sulfur-doped Fe/N/C nanosheets as highly efficient electrocatalysts for oxygen reduction reaction, ACS Appl. Mater. Interfaces 8 (2016) 19379–19385, https://doi.org/10.1021/acsami.6b02078.

[120] X. Liu, L. Xu, G. Xu, W. Jia, Y. Ma, Y. Zhang, Selective hydrodeoxygenation of lignin-derived phenols to cyclohexanols or cyclohexanes over magnetic CoNx@ NC catalysts under mild conditions, ACS Catal. 6 (2016) 7611–7620, https://doi.org/10.1021/acscatal.6b01785.

[121] R.V. Jagadeesh, K. Murugesan, A.S. Alshammari, H. Neumann, M.-M. Pohl, J. Radnik, M. Beller, MOF-derived cobalt nanoparticles catalyze a general synthesis of amines, Science 358 (2017) 326–332, https://doi.org/10.1126/science.aan6245.

[122] P. Su, H. Xiao, J. Zhao, Y. Yao, Z. Shao, C. Li, Q. Yang, Nitrogen-doped carbon nanotubes derived from Zn–Fe-ZIF nanospheres and their application as efficient oxygen reduction electrocatalysts with in situ generated iron species, Chem. Sci. 4 (2013), 2941, https://doi.org/10.1039/c3sc51052b.

[123] G. Zhang, Y. Jia, C. Zhang, X. Xiong, K. Sun, R. Chen, W. Chen, Y. Kuang, L. Zheng, H. Tang, W. Liu, J. Liu, X. Sun, W.-F. Lin, H. Dai, A general route via formamide condensation to prepare atomically dispersed metal–nitrogen–carbon electrocatalysts for energy technologies, Energy Environ. Sci. 12 (2019) 1317–1325, https://doi.org/10.1039/C9EE00162J.

[124] X. Wang, J. Wang, D. Wang, S. Dou, Z. Ma, J. Wu, L. Tao, A. Shen, C. Ouyang, Q. Liu, S. Wang, One-pot synthesis of nitrogen and sulfur co-doped graphene as efficient metal-free electrocatalysts for the oxygen reduction reaction, Chem. Commun. 50 (2014) 4839–4842, https://doi.org/10.1039/C4CC00440J.

[125] L. Sun, L. Wang, C. Tian, T. Tan, Y. Xie, K. Shi, M. Li, H. Fu, Nitrogen-doped graphene with high nitrogen level via a one-step hydrothermal reaction of graphene oxide with urea for superior capacitive energy storage, RSC Adv. 2 (2012), 4498, https://doi.org/10.1039/c2ra01367c.

[126] J. Li, B. Shen, Z. Hong, B. Lin, B. Gao, Y. Chen, A facile approach to synthesize novel oxygen-doped g-C3N4 with superior visible-light photoreactivity, Chem. Commun. 48 (2012), 12017, https://doi.org/10.1039/c2cc35862j.

[127] S. Fujita, H. Watanabe, A. Katagiri, H. Yoshida, M. Arai, Nitrogen and oxygen-doped metal-free carbon catalysts for chemoselective transfer hydrogenation of nitrobenzene, styrene, and 3-nitrostyrene with hydrazine, J. Mol. Catal. A Chem. 393 (2014) 257–262, https://doi.org/10.1016/j.molcata.2014.06.021.

[128] X. Sun, P. Song, T. Chen, J. Liu, W. Xu, Fluorine-doped BP 2000: highly efficient metal-free electrocatalysts for acidic oxygen reduction reaction with superlow H2O2 yield, Chem. Commun. 49 (2013), 10296, https://doi.org/10.1039/c3cc45480k.

[129] M.B. Gumpu, G.K. Mani, N. Nesakumar, A.J. Kulandaisamy, K.J. Babu, J.B. B. Rayappan, Electrocatalytic nanocauliflower structured fluorine doped CdO thin film as a potential arsenic sensor, Sens. Actuators B 234 (2016) 426–434, https://doi.org/10.1016/j.snb.2016.05.011.

[130] S.G. Peera, A. Arunchander, A.K. Sahu, Cumulative effect of transition metals on nitrogen and fluorine co-doped graphite nanofibers: an efficient and highly durable non-precious metal catalyst for the oxygen reduction reaction, Nanoscale 8 (2016) 14650–14664, https://doi.org/10.1039/C6NR02263D.

[131] K. Zhao, Y. Su, X. Quan, Y. Liu, S. Chen, H. Yu, Enhanced H2O2 production by selective electrochemical reduction of O2 on fluorine-doped hierarchically porous carbon, J. Catal. 357 (2018) 118–126, https://doi.org/10.1016/j.jcat.2017.11.008.

[132] J. Xie, X. Zhao, M. Wu, Q. Li, Y. Wang, J. Yao, Metal-free fluorine-doped carbon electrocatalyst for CO2 reduction outcompeting hydrogen evolution, Angew. Chem. Int. Ed. 57 (2018) 9640–9644, https://doi.org/10.1002/anie.201802055.

[133] F. Herold, J. Gläsel, B.J.M. Etzold, M. Rønning, Can temperature-programmed techniques provide the gold standard for carbon surface characterization? Chem. Mater. 34 (2022) 8490–8516, https://doi.org/10.1021/acs.chemmater.2c02449.

[134] D. Formenti, F. Ferretti, F.K. Scharnagl, M. Beller, Reduction of nitro compounds using 3d-non-noble metal catalysts, Chem. Rev. 119 (2019) 2611–2680, https://doi.org/10.1021/acs.chemrev.8b00547.

[135] A. Li, S.A. Nicolae, M. Qiao, K. Preuss, P.A. Szilágyi, A. Moores, M.-M. Titirici, Homogenous meets heterogenous and electro-catalysis: iron-nitrogen molecular complexes within carbon materials for catalytic applications, ChemCatChem 11 (2019) 3602–3625, https://doi.org/10.1002/cctc.201900910.

[136] R.V. Jagadeesh, K. Natte, H. Junge, M. Beller, Nitrogen-doped graphene-activated iron-oxide-based nanocatalysts for selective transfer hydrogenation of nitroarenes, ACS Catal. 5 (2015) 1526–1529, https://doi.org/10.1021/cs501916p.

[137] J. Chen, Y. Yao, J. Zhao, Y. Zhao, Y. Zheng, M. Li, Q. Yang, A highly active non-precious metal catalyst based on Fe–N–C@CNTs for nitroarene reduction, RSC Adv. 6 (2016) 96203–96209, https://doi.org/10.1039/C6RA20666B.

[138] J. Shi, Y. Wang, W. Du, Z. Hou, Synthesis of graphene encapsulated Fe3C in carbon nanotubes from biomass and its catalysis application, Carbon 99 (2016) 330–337, https://doi.org/10.1016/j.carbon.2015.12.049.

[139] F. Schüth, M.D. Ward, J.M. Buriak, Common pitfalls of catalysis manuscripts submitted to chemistry of materials, Chem. Mater. 30 (2018) 3599–3600, https://doi.org/10.1021/acs.chemmater.8b01831.

[140] S. Xu, D. Yu, S. Liao, T. Ye, H. Sheng, Nitrogen-doped carbon supported iron oxide as efficient catalysts for chemoselective hydrogenation of nitroarenes, RSC Adv. 6 (2016) 96431–96435, https://doi.org/10.1039/C6RA18935K.

[141] Y. Duan, X. Dong, Z. Wang, J. Xiao, Y. Yuan, Y. Yang, Hydrogenation of functionalized nitroarenes catalyzed by single-phase pyrite FeS2 nanoparticles on N, S-codoped porous carbon, ChemSusChem 12 (2019) 4636–4644, https://doi.org/10.1002/cssc.201901867.

[142] Y. Li, Y.-X. Zhou, X. Ma, H.-L. Jiang, A metal–organic framework-templated synthesis of γ-Fe 2 O 3 nanoparticles encapsulated in porous carbon for efficient

and chemoselective hydrogenation of nitro compounds, Chem. Commun. 52 (2016) 4199–4202, https://doi.org/10.1039/C6CC00011H.

[143] T. Kitanosono, S. Kobayashi, Reactions in water involving the "on-water" mechanism, Chem. Eur. J. 26 (2020) 9408–9429, https://doi.org/10.1002/chem.201905482.

[144] Z. Wei, J. Wang, S. Mao, D. Su, H. Jin, Y. Wang, F. Xu, H. Li, Y. Wang, In situ-generated Co^0 -Co_3O_4 /N-doped carbon nanotubes hybrids as efficient and chemoselective catalysts for hydrogenation of nitroarenes, ACS Catal. 5 (2015) 4783–4789, https://doi.org/10.1021/acscatal.5b00737.

[145] S. Yang, L. Peng, D.T. Sun, E. Oveisi, S. Bulut, W.L. Queen, Metal–organic-framework-derived Co3S4 hollow nanoboxes for the selective reduction of nitroarenes, ChemSusChem 11 (2018) 3131–3138, https://doi.org/10.1002/cssc.201801641.

[146] H. Guo, R. Gao, M. Sun, H. Guo, B. Wang, L. Chen, Cobalt entrapped in N, S-codoped porous carbon: catalysts for transfer hydrogenation with formic acid, ChemSusChem 12 (2019) 487–494, https://doi.org/10.1002/cssc.201802392.

[147] M. Yuan, Y. Long, J. Yang, X. Hu, D. Xu, Y. Zhu, Z. Dong, Biomass sucrose-derived cobalt@nitrogen-doped carbon for catalytic transfer hydrogenation of nitroarenes with formic acid, ChemSusChem 11 (2018) 4156–4165, https://doi.org/10.1002/cssc.201802163.

[148] B. Sahoo, D. Formenti, C. Topf, S. Bachmann, M. Scalone, K. Junge, M. Beller, Biomass-derived catalysts for selective hydrogenation of nitroarenes, ChemSusChem 10 (2017) 3035–3039, https://doi.org/10.1002/cssc.201700796.

[149] Y. Duan, T. Song, X. Dong, Y. Yang, Enhanced catalytic performance of cobalt nanoparticles coated with a N, P-codoped carbon shell derived from biomass for transfer hydrogenation of functionalized nitroarenes, Green Chem. 20 (2018) 2821–2828, https://doi.org/10.1039/C8GC00619A.

[150] T. Schwob, M. Ade, R. Kempe, A cobalt catalyst permits the direct hydrogenative synthesis of 1H-perimidines from a dinitroarene and an aldehyde, ChemSusChem 12 (2019) 3013–3017, https://doi.org/10.1002/cssc.201900498.

[151] F. Chen, B. Sahoo, C. Kreyenschulte, H. Lund, M. Zeng, L. He, K. Junge, M. Beller, Selective cobalt nanoparticles for catalytic transfer hydrogenation of N-heteroarenes, Chem. Sci. 8 (2017) 6239–6246, https://doi.org/10.1039/C7SC02062G.

[152] Z. Wei, Y. Chen, J. Wang, D. Su, M. Tang, S. Mao, Y. Wang, Cobalt encapsulated in N-doped graphene layers: an efficient and stable catalyst for hydrogenation of quinoline compounds, ACS Catal. 6 (2016) 5816–5822, https://doi.org/10.1021/acscatal.6b01240.

[153] G. Li, H. Yang, H. Zhang, Z. Qi, M. Chen, W. Hu, L. Tian, R. Nie, W. Huang, Encapsulation of nonprecious metal into ordered mesoporous N-doped carbon for efficient quinoline transfer hydrogenation with formic acid, ACS Catal. 8 (2018) 8396–8405, https://doi.org/10.1021/acscatal.8b01404.

[154] F.K. Scharnagl, M.F. Hertrich, F. Ferretti, C. Kreyenschulte, H. Lund, R. Jackstell, M. Beller, Hydrogenation of terminal and internal olefins using a biowaste-derived heterogeneous cobalt catalyst, Sci. Adv. 4 (2018) eaau1248, https://doi.org/10.1126/sciadv.aau1248.

[155] J. Long, Y. Zhou, Y. Li, Transfer hydrogenation of unsaturated bonds in the absence of base additives catalyzed by a cobalt-based heterogeneous catalyst, Chem. Commun. 51 (2015) 2331–2334, https://doi.org/10.1039/C4CC08946D.

[156] J. Long, K. Shen, Y. Li, Bifunctional N-doped Co@C catalysts for base-free transfer hydrogenations of nitriles: controllable selectivity to primary amines vs imines, ACS Catal. 7 (2017) 275–284, https://doi.org/10.1021/acscatal.6b02327.

[157] Z. Yuan, B. Liu, P. Zhou, Z. Zhang, Q. Chi, Preparation of nitrogen-doped carbon supported cobalt catalysts and its application in the reductive amination, J. Catal. 370 (2019) 347–356, https://doi.org/10.1016/j.jcat.2019.01.004.

[158] T. Senthamarai, K. Murugesan, N. Natte, N.V. Kalevaru, H. Neumann, P.C.J. Kamer, R.V. Jagadeesh, Expedient synthesis of N-methyl- and N-alkylamines by reductive amination using reusable cobalt oxide nanoparticles, ChemCatChem 10 (2018) 1235–1240, https://doi.org/10.1002/cctc.201701617.

[159] J. Piera, J.-E. Bäckvall, Catalytic oxidation of organic substrates by molecular oxygen and hydrogen peroxide by multistep electron transfer—A biomimetic approach, Angew. Chem. Int. Ed. 47 (2008) 3506–3523, https://doi.org/10.1002/anie.200700604.

[160] B. Chen, L. Wang, S. Gao, Recent advances in aerobic oxidation of alcohols and amines to imines, ACS Catal. 5 (2015) 5851–5876, https://doi.org/10.1021/acscatal.5b01479.

[161] K. Sun, H. Shan, H. Neumann, G.-P. Lu, M. Beller, Efficient iron single-atom catalysts for selective ammoxidation of alcohols to nitriles, Nat Commun. 13 (2022), 1848, https://doi.org/10.1038/s41467-022-29074-1.

[162] T. Senthamarai, V.G. Chandrashekar, N. Rockstroh, J. Rabeah, S. Bartling, R.V. Jagadeesh, M. Beller, A "universal" catalyst for aerobic oxidations to synthesize (hetero)aromatic aldehydes, ketones, esters, acids, nitriles, and amides, Chem 8 (2022) 508–531, https://doi.org/10.1016/j.chempr.2021.12.001.

[163] A.V. Iosub, S.S. Stahl, Catalytic aerobic dehydrogenation of nitrogen heterocycles using heterogeneous cobalt oxide supported on nitrogen-doped carbon, Org. Lett. 17 (2015) 4404–4407, https://doi.org/10.1021/acs.orglett.5b01790.

[164] J. Xie, K. Yin, A. Serov, K. Artyushkova, H.N. Pham, X. Sang, R.R. Unocic, P. Atanassov, A.K. Datye, R.J. Davis, Selective aerobic oxidation of alcohols over atomically-dispersed non-precious metal catalysts, ChemSusChem 10 (2017) 359–362, https://doi.org/10.1002/cssc.201601364.

[165] W.C. Howland, J.B. Gerken, S.S. Stahl, Y. Surendranath, Thermal hydroquinone oxidation on Co/N-doped carbon proceeds by a band-mediated electrochemical mechanism, J. Am. Chem. Soc. 144 (2022) 11253–11262, https://doi.org/10.1021/jacs.2c02746.

[166] J.S. Bates, S. Biswas, S.-E. Suh, M.R. Johnson, B. Mondal, T.W. Root, S.S. Stahl, Chemical and electrochemical O2 reduction on earth-abundant M-N-C catalysts

[167] J. Ryu, D.T. Bregante, W.C. Howland, R.P. Bisbey, C.J. Kaminsky, Y. Surendranath, Thermochemical aerobic oxidation catalysis in water can be analysed as two coupled electrochemical half-reactions, Nat Catal. 4 (2021) 742–752, https://doi.org/10.1038/s41929-021-00666-2.

[168] K. Ping, M. Alam, M. Käärik, J. Leis, N. Kongi, I. Järving, P. Starkov, Surveying iron-organic framework TAL-1-derived materials in ligandless heterogeneous oxidative catalytic transformations of alkylarenes, Synlett 30 (2019) 1536–1540, https://doi.org/10.1055/s-0037-1611877.

[169] K. Ping, A. Braschinsky, M. Alam, R. Bhadoria, V. Mikli, A. Mere, J. Aruväli, P. Paiste, S. Vlassov, M. Kook, M. Rähn, V. Sammelselg, K. Tammeveski, N. Kongi, P. Starkov, Fused hybrid linkers for metal-organic framework-derived bifunctional oxygen electrocatalysts, ACS Appl. Energy Mater. 3 (2020) 152–157, https://doi.org/10.1021/acsaem.9b02039.

[170] T. Song, X. Zhou, X. Wang, J. Xiao, Y. Yang, One-pot cascade synthesis of α-diketones from aldehydes and ketones in water by using a bifunctional iron nanocomposite catalyst, Green Chem. 23 (2021) 1955–1959, https://doi.org/10.1039/D0GC03739G.

[171] R.V. Jagadeesh, H. Junge, M.-M. Pohl, J. Radnik, A. Brückner, M. Beller, Selective oxidation of alcohols to esters using heterogeneous Co3O4–N@C catalysts under mild conditions, J. Am. Chem. Soc. 135 (2013) 10776–10782, https://doi.org/10.1021/ja403615c.

[172] X.-H. Li, M. Antonietti, Metal nanoparticles at mesoporous N-doped carbons and carbon nitrides: functional Mott-Schottky heterojunctions for catalysis, Chem. Soc. Rev. 42 (2013) 6593, https://doi.org/10.1039/c3cs60067j.

[173] Y.-X. Zhou, Y.-Z. Chen, L. Cao, J. Lu, H.-L. Jiang, Conversion of a metal–organic framework to N-doped porous carbon incorporating Co and CoO nanoparticles: direct oxidation of alcohols to esters, Chem. Commun. 51 (2015) 8292–8295, https://doi.org/10.1039/C5CC01588J.

[174] F. Xie, Q.-H. Chen, R. Xie, H.-F. Jiang, M. Zhang, MOF-derived nanocobalt for oxidative functionalization of cyclic amines to quinazolinones with 2-aminoarylmethanols, ACS Catal. 8 (2018) 5869–5874, https://doi.org/10.1021/acscatal.8b01366.

[175] P. Yin, T. Yao, Y. Wu, L. Zheng, Y. Lin, W. Liu, H. Ju, J. Zhu, X. Hong, Z. Deng, G. Zhou, S. Wei, Y. Li, Single cobalt atoms with precise N-coordination as superior oxygen reduction reaction catalysts, Angew. Chem. Int. Ed. 55 (2016) 10800–10805, https://doi.org/10.1002/anie.201604802.

[176] K. Ping, M. Alam, S.R. Kahnert, R. Bhadoria, A. Mere, V. Mikli, M. Käärik, J. Aruväli, P. Paiste, A. Kikas, V. Kisand, I. Järving, J. Leis, N. Kongi, P. Starkov, Multi-purpose heterogeneous catalyst material from an amorphous cobalt metal–organic framework, Mater. Adv. 2 (2021) 4009–4015, https://doi.org/10.1039/D1MA00414J.

[177] C. Bai, A. Li, X. Yao, H. Liu, Y. Li, Efficient and selective aerobic oxidation of alcohols catalysed by MOF-derived Co catalysts, Green Chem. 18 (2016) 1061–1069, https://doi.org/10.1039/C5GC02082D.

[178] A. Sarkar, D. Formenti, F. Ferretti, C. Kreyenschulte, S. Bartling, K. Junge, M. Beller, F. Ragaini, Iron/N-doped graphene nano-structured catalysts for general cyclopropanation of olefins, Chem. Sci. 11 (2020) 6217–6221, https://doi.org/10.1039/D0SC01650K.

[179] J. He, A. Dhakshinamoorthy, A. Primo, H. Garcia, Iron nanoparticles embedded in graphitic carbon matrix as heterogeneous catalysts for the oxidative C–N coupling of aromatic N–H compounds and amides, ChemCatChem 9 (2017) 3003–3012, https://doi.org/10.1002/cctc.201700429.

[180] L. Zhang, A. Wang, W. Wang, Y. Huang, X. Liu, S. Miao, J. Liu, T. Zhang, Co–N–C catalyst for C-C coupling reactions: on the catalytic performance and active sites, ACS Catal. 5 (2015) 6563–6572, https://doi.org/10.1021/acscatal.5b01223.

[181] R. Xie, F. Xie, C.-J. Zhou, H.-F. Jiang, M. Zhang, Hydrogen transfer-mediated selective dual C-H alkylations of 2-alkylquinolines by doped TiO2-supported nanocobalt oxides, J. Catal. 377 (2019) 449–454, https://doi.org/10.1016/j.jcat.2019.07.058.

[182] J. Li, J. Liu, J. Zhang, T. Wan, L. Huang, X. Wang, R. Pan, Z. An, D.G. Vlachos, An unconventional DCOx favored Co/N-C catalyst for efficient conversion of fatty acids and esters to liquid alkanes, Appl. Catal. A 591 (2020), 117385, https://doi.org/10.1016/j.apcata.2019.117385.

[183] B. Sahoo, A.-E. Surkus, M.-M. Pohl, J. Radnik, M. Schneider, S. Bachmann, M. Scalone, K. Junge, M. Beller, A biomass-derived non-noble cobalt catalyst for selective hydrodehalogenation of alkyl and (hetero)aryl halides, Angew. Chem. Int. Ed. 56 (2017) 11242–11247, https://doi.org/10.1002/anie.201702478.

[184] X. Cui, W. Li, K. Junge, Z. Fei, M. Beller, P.J. Dyson, Selective acceptorless dehydrogenation of primary amines to imines by core-shell cobalt nanoparticles, Angew. Chem. Int. Ed. 59 (2020) 7501–7507, https://doi.org/10.1002/anie.201915526.

[185] S. Pisiewicz, D. Formenti, A.-E. Surkus, M.-M. Pohl, J. Radnik, K. Junge, C. Topf, S. Bachmann, M. Scalone, M. Beller, Synthesis of nickel nanoparticles with N-doped graphene shells for catalytic reduction reactions, ChemCatChem 8 (2016) 129–134, https://doi.org/10.1002/cctc.201500848.

[186] G. Hahn, P. Kunnas, N. de Jonge, R. Kempe, General synthesis of primary amines via reductive amination employing a reusable nickel catalyst, Nat. Catal. 2 (2019) 71–77, https://doi.org/10.1038/s41929-018-0202-6.

[187] F. Yang, M. Wang, W. Liu, B. Yang, Y. Wang, J. Luo, Y. Tang, L. Hou, Y. Li, Z. Li, B. Zhang, W. Yang, Y. Li, Atomically dispersed Ni as the active site towards selective hydrogenation of nitroarenes, Green Chem. 21 (2019) 704–711, https://doi.org/10.1039/C8GC03664K.

[188] Y. Zhang, H. Yang, Q. Chi, Z. Zhang, Nitrogen-doped carbon-supported nickel nanoparticles: A robust catalyst to bridge the hydrogenation of nitriles and the

reductive amination of carbonyl compounds for the synthesis of primary amines, ChemSusChem 12 (2019) 1246–1255, https://doi.org/10.1002/cssc.201802459.

[189] G. Gao, P. Sun, Y. Li, F. Wang, Z. Zhao, Y. Qin, F. Li, Highly stable porous-carbon-coated Ni catalysts for the reductive amination of levulinic acid via an unconventional pathway, ACS Catal. 7 (2017) 4927–4935, https://doi.org/10.1021/acscatal.7b01786.

[190] D. Liu, L. Zhang, W. Han, M. Tang, L. Zhou, Y. Zhang, X. Li, Z. Qin, H. Yang, One-step fabrication of Ni-embedded hierarchically-porous carbon microspheres for levulinic acid hydrogenation, Chem. Eng. J. 369 (2019) 386–393, https://doi.org/10.1016/j.cej.2019.03.072.

[191] B. Yu, J.-N. Xie, C.-L. Zhong, W. Li, L.-N. He, Copper(I)@carbon-catalyzed carboxylation of terminal alkynes with CO_2 at atmospheric pressure, ACS Catal. 5 (2015) 3940–3944, https://doi.org/10.1021/acscatal.5b00764.

[192] W. Sun, L. Gao, X. Sun, G. Zheng, A novel route with a Cu(II)-MOF-derived structure to synthesize Cu/Cu$_2$O NPs@graphene: the electron transfer leads to the synergistic effect of the Cu(0)–Cu(I) phase for an effective catalysis of the Sonogashira cross-coupling reactions, Dalton Trans. 47 (2018) 5538–5541, https://doi.org/10.1039/C8DT00465J.

[193] A.K. Kar, R. Srivastava, Selective synthesis of Cu–Cu$_2$O/C and CuO–Cu$_2$O/C catalysts for Pd-free C-C, C–N coupling and oxidation reactions, Inorg. Chem. Front. 6 (2019) 576–589, https://doi.org/10.1039/C8QI01198B.

[194] W. Li, X. Cui, K. Junge, A.-E. Surkus, C. Kreyenschulte, S. Bartling, M. Beller, General and chemoselective copper oxide catalysts for hydrogenation reactions, ACS Catal. 9 (2019) 4302–4307, https://doi.org/10.1021/acscatal.8b04807.

[195] B. Liu, H. Yao, W. Song, L. Jin, I.M. Mosa, J.F. Rusling, S.L. Suib, J. He, Ligand-free noble metal nanocluster catalysts on carbon supports via "soft" nitriding, J. Am. Chem. Soc. 138 (2016) 4718–4721, https://doi.org/10.1021/jacs.6b01702.

[196] B. Liu, P. Wang, A. Lopes, L. Jin, W. Zhong, Y. Pei, S.L. Suib, J. He, Au–carbon electronic interaction mediated selective oxidation of styrene, ACS Catal. 7 (2017) 3483–3488, https://doi.org/10.1021/acscatal.7b01048.

[197] J.L. Fiorio, R.V. Gonçalves, E. Teixeira-Neto, M.A. Ortuño, N. López, L.M. Rossi, Accessing frustrated lewis pair chemistry through robust gold@N-doped carbon for selective hydrogenation of alkynes, ACS Catal. 8 (2018) 3516–3524, https://doi.org/10.1021/acscatal.8b00806.

[198] X. Li, Y. Pan, H. Yi, J. Hu, D. Yang, F. Lv, W. Li, J. Zhou, X. Wu, A. Lei, L. Zhang, Mott-Schottky effect leads to alkyne semihydrogenation over Pd-nanocube@N-doped carbon, ACS Catal. 9 (2019) 4632–4641, https://doi.org/10.1021/acscatal.9b01001.

[199] L.M. Martínez-Prieto, M. Puche, C. Cerezo-Navarrete, B. Chaudret, Uniform Ru nanoparticles on N-doped graphene for selective hydrogenation of fatty acids to alcohols, J. Catal. 377 (2019) 429–437, https://doi.org/10.1016/j.jcat.2019.07.040.

[200] B. Guo, H.-X. Li, S.-Q. Zhang, D.J. Young, J.-P. Lang, C-N bond formation catalyzed by ruthenium nanoparticles supported on N-doped carbon via acceptorless dehydrogenation to secondary amines, imines, benzimidazoles and quinoxalines, ChemCatChem 10 (2018) 5627–5636, https://doi.org/10.1002/cctc.201801525.

[201] Y. Liu, X. Yang, H. Liu, Y. Ye, Z. Wei, Nitrogen-doped mesoporous carbon supported Pt nanoparticles as a highly efficient catalyst for decarboxylation of saturated and unsaturated fatty acids to alkanes, Appl. Catal. B 218 (2017) 679–689, https://doi.org/10.1016/j.apcatb.2017.06.065.

[202] X. Guo, C. Yu, Z. Yin, S. Sun, C.T. Seto, Hydrodehalogenation of polyhalogenated aromatics catalyzed by NiPd nanoparticles supported on nitrogen-doped graphene, ChemSusChem 11 (2018) 1617–1620, https://doi.org/10.1002/cssc.201800289.